UNIVERSITY OF CALIFORNIA
RIVERSIDE

A Streamlined Route to Synthesize $LiFePO_4$/C in an Unrestricted Environment

A Dissertation submitted in partial satisfaction
of the requirements for the degree of

Doctor of Philosophy

in

Materials Science and Engineering

by

Fei Gu

March 2020

Dissertation Committee:
Dr. Alfredo A. Martinez-Morales, Chairperson
Dr. Juchen Guo
Dr. Reza Abbaschian

The Dissertation of Fei Gu is approved:

_____

_____

_____

Committee Chairperson

University of California, Riverside

`

ABSTRACT OF THE DISSERTATION

A Streamlined Route to Synthesize $LiFePO_4$/C in an Unrestricted Environment

by

Fei Gu

Doctor of Philosophy, Graduate Program in Materials Science and Engineering
University of California, Riverside, March 2020
Dr. Alfredo A. Martinez-Morales, Chairperson

In this dissertation, a practical and streamlined route for the synthesis of carbonized lithium iron phosphate ($LiFePO_4$, LFP) is developed via a solid state-based lithiation process performed under an unrestricted environment. Extensive characterization and analysis are performed to study the reaction mechanism, crystallinity of synthesized product, oxidation protection during synthesis reaction, carbonization of LFP, and synthesis scale-up.

The main motivation of this work is to achieve good quality carbonized LFP product, by minimizing the oxidation of LFP during synthesis, while combining the synthesis and carbonization of LFP into a single step process. Chapter 1 introduces the background of Li-ion battery, commercialized cathode materials, and the approaches developed for LFP synthesis. In Chapter 2, well-crystallized LFP is synthesized via a solid state-based lithiation process using lithium acetate ($C_2H_3LiO_2$) and iron phosphate ($FePO_4$) as starting materials. Two key findings are identified for achieving good crystalline LFP in an unrestricted environment synthesis: 1) using quartz $FePO_4$ (rather than amorphous $FePO_4$) thermodynamically activates and accelerates the LFP synthesis reaction; and, 2) $C_2H_3LiO_2$

`

in liquid state accelerates the lithiation process by increasing the uniformity of mixing and contact surface area between particles during lithiation. Compared to conventional solid state synthesis, the required synthesis time is significantly reduced from several hours down to 30 minutes. In Chapter 3, a carbon source (i.e. gelatin) is added as a sacrificial material to help inhibit the oxidation of LFP by 1) reacting and consuming part of the oxygen in the environment; and, 2) acting as a reducing agent for oxidized LFP. The thermal decomposition process of the carbon source, starting at the low temperature range, is investigated to understand its critical role in inhibiting LFP oxidation during reaction. Highly crystalline LFP is successfully synthesized by oxidation protection. In Chapter 4, an auto pressure release method for scaling-up and streamlined synthesis process is developed to auto-release the increased inner pressure caused by the gaseous byproducts during LFP synthesis. To further improve the quality of LFP, water is used as a sacrificial material to deoxygenate the reaction system and protect LFP from oxidation. The step-by-step development of a streamlined synthesis process for carbonized LFP with good quality is successfully achieved. In Chapter 5, the developmental evolution of this approach and the resolved issues through this dissertation are summarized and discussed.

`

Table of Contents

`

`

List of Figures

`

List of Tables

`

Chapter 1 Introduction

1.1 Lithium-ion Battery

Rechargeable battery is named by their ability to be charged and discharged for many times in compare to disposable or primary battery [1]. Among different types of rechargeable battery, Li-ion battery (LIB) is the most widely used, especially in portable electronic devices, electric vehicle, and unmanned aerial vehicle [2]. As demonstrated in Figure 1.1, in compare to other commonly used batteries that contain heavy metal elements, such as Ni-MH [3], Ni-Cd [4], and Lead Acid battery [5], LIB is featured by high volumetric energy density and high specific energy density [6]. Therefore, it is smaller on size and lighter on weight which make it perfect for energy storage with limited volume and weight. Also, LIB has a long cycle of life and able to be environmental friendliness.

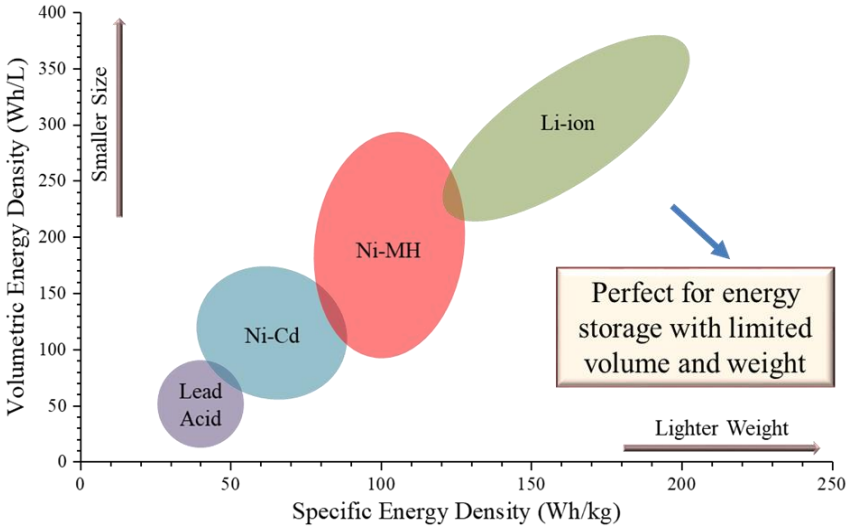

Figure 1.1. Comparation of volumetric energy density and specific energy density for Lithium-ion, Ni-MH, Ni-Cd, and Lead Acid battery

The schematic diagram of the working mechanism for Lithium-ion battery is illustrated in Figure 1.2 [7]. A LIB full cell contains two electrodes, a cathode and an anode. The two electrodes are separated by a porous separator and filled with liquid electrolyte. Cathode, which is usually lithium metal oxide, perform a role of lithium ion (Li^+) donor during charging. Li^+ migrates from cathode to anode under the force of electric field. Simultaneously, electrons that generated from cathode pass through the external circuit to reach anode. Li^+ inserted into the anode recombines with electron and so stored in the anode side. On the other hand, while discharging, Li^+ is extracted form anode and diffuse back to the cathode side. This time, electrons pass through the external circuit to reach cathode. And the current flow generated in this process is utilized to do the work for connected electronic device [8].

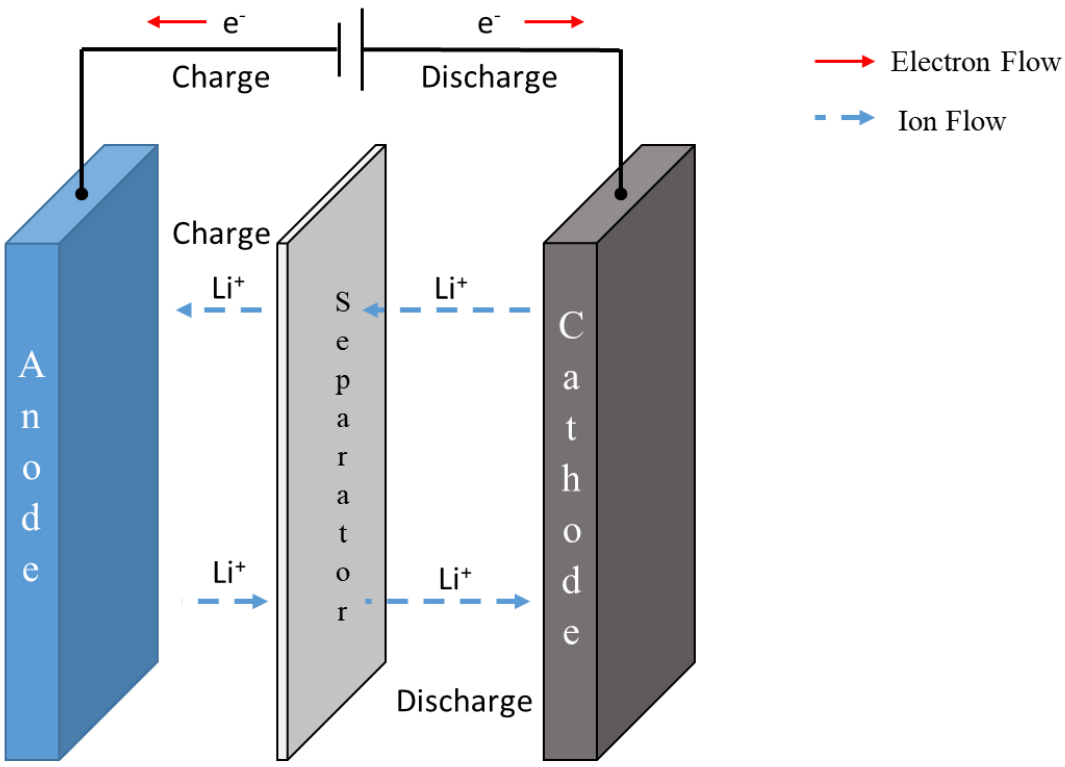

Figure 1.2. Schematic diagram of the working mechanism of a lithium ion battery

`

Although all components play their important role, cathode is always the most critical part for a LIB. This is because the capacity and working voltage window are mainly depended on the structure and type of cathode used [8]. And the electronic conductivity and ionic conductivity of cathode significantly impact the high rate performance of the LIB [9]. Also, half the cost of battery manufacturing is related to cathode material processing [10]. Furthermore, since cathode materials usually contain oxygen element and decompose when thermal failure happen, oxygen may be released and fire can be caught in this case. Thus cathode materials are also related to the safety of LIB [11].

1.2 Lithium iron phosphate

Table 1.1 is the characteristics of Li-ion battery cathode materials [12]. Five materials, $LiCoO_2$, $LiNi_{0.8}Co_{0.15}Al_{0.05}O_2$, $LiNi_{1/3}Co_{1/3}Mn_{1/3}O_2$, $LiMN_2O_4$, and $LiFePO_4$, are included. These five materials are compared because they have all been commercially used. They can be divided into three group by structure: (1) LCO, NCA and NMC have a layered oxides structure; (2) LMO has a spinel oxide structure; and (3) LFP has an olivine structure. This dissertation is focus on the study of the last one, LFP.

`

Table 1.1. Characteristics of Li-ion battery cathode materials

	Potential versus Li/Li+, V	Specific capacity, mAh/g	Toxicity	Thermal stability
$LiCoO_2$ (LCO)	3.9	140	Toxic	Acceptable
$LiNi_{0.8}Co_{0.15}Al_{0.05}O_2$ (NCA)	3.8	180-200	Toxic	Acceptable
$LiNi_{1/3}Co_{1/3}Mn_{1/3}O_2$ (NMC)	3.8	160-170	Toxic	Acceptable
$LiMn_2O_4$ (LMO)	4.1	100-120	Toxic	Poor
$LiFePO_4$ (LFP)	3.45	150-170	Non-toxic	Best

`

The crystal structure of LFP is shown in Figure 1.3 [13]. It belongs to the olivine family of lithium ortho-phosphates with an orthorhombic lattice structure in the space group Pnma [14], [15]. In the lattice, Li, Fe, and P atoms occupying octahedral 4a, octahedral 4c, and tetrahedral 4c sites, respectively. Oxygen atoms are in a slightly distorted, hexagonal close-packed arrangement. The FeO_6 octahedra share common corners in the bc plane, and LiO_6 octahedra form a linear edge-shared chain parallel to the b direction. A FeO_6 octahedron shares edges with two LiO_6 octahedra and one PO_4 tetrahedron [16].

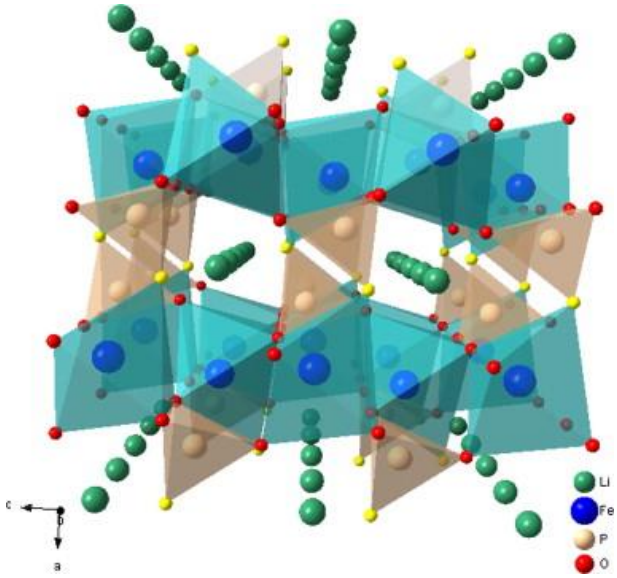

Figure 1.3. The structure of olivine type $LiFePO_4$, viewed along the b-axis

LFP has an excellent specific capacity which is able to approach its theoretical capacity, 170 mAh/g. Among other four commercially used cathode, the materials that can match LFP in capacity are NCA and NMC. LFP has the lowest working voltage among five cathode materials. However, LFP has better discharge profile. As illustrate in Figure 1.3, in compare to the layered oxides NMC and spinel oxide LMO, olivine LFP has a flat

`

discharge plateau [17]. A 2D diffusion mechanism has been proposed to explain the process of insertion Li^+ into cathode during discharge [18], [19]. A simple shrinking core model was proposed later by Venkat Srinivasan and John Newman [20]. Then Delams *et al.*, proposed a domino-cascade model [21]. So far, there is still no single model that can depict the lithation/delithation process in $LiFePO_4$ [22]. However, it is do believed that the flat discharge plateau is contributed by its olivine structure.

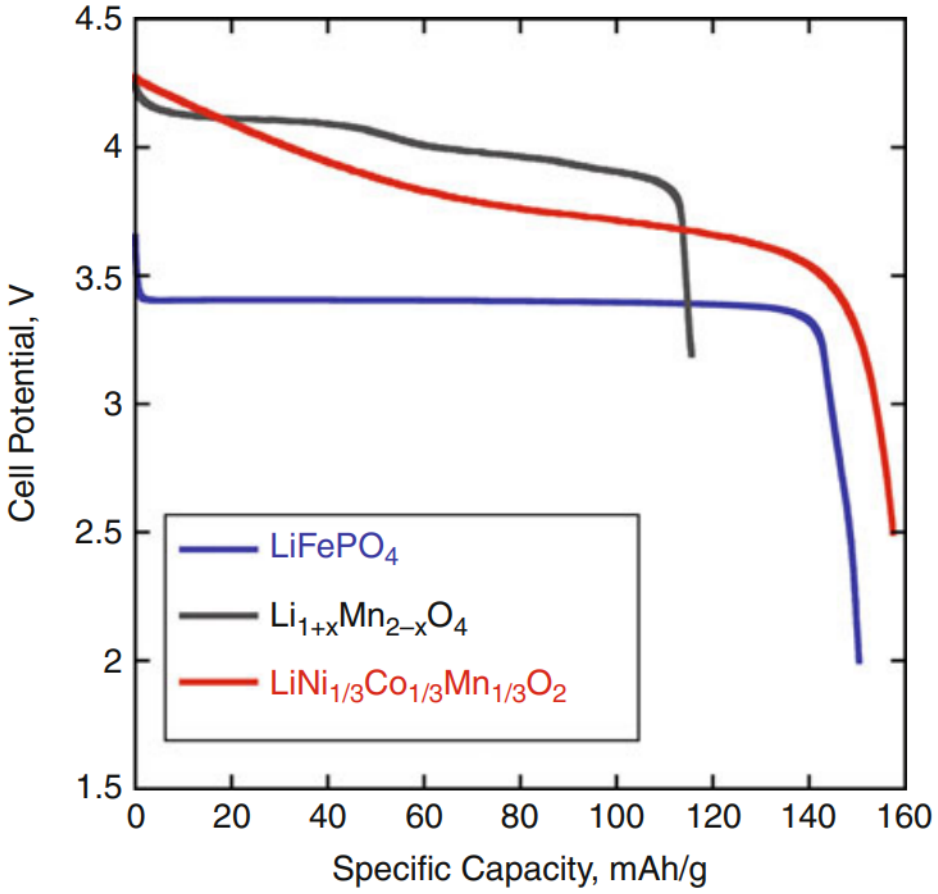

Figure 1.4. The discharge profile of LFP, LMO and NMC based LIBs.

`

The olivine structure also makes a great contribution to the magnificent thermal stability of LFP. LFP is the most stable materials at high temperatures among commercially used cathodes. This is because Fe atoms are strongly bonded with PO_4 tetrahedron [17]. $LiFePO_4$ is stable up to 400 °C, while cathode with layer oxide structure and spinel oxide structure starts to decompose around 250 °C [23], [24]. Also, due to a stronger bond between O atoms and P atoms, PO_4 tetrahedron is more stable than LFP. Therefore, no O_2 gas will be released even LFP starts to decompose. This significantly decreases the risk of catching fire for LFP based LIBs [25]. On the other hand, olivine structure, because of the high lattice stability, also contributes to the excellent cyclic performance of LFP [26]. LFP reacts very slow with electrolyte and so have a very long cycle of life [27]. And with the features mentioned above, LFP is able to operate safely with long time of using.

LFP is also non-toxic and environmentally friendly because it is based on Fe element. In contrast, both layer oxide cathode (LCO, NCA, NMC) and spinel oxide cathode (LMO) have the issue of using heavy metal elements (Co, Ni, Mn). This creates a contradiction, except LFP, that although LIB is regarded as the solution of green energy, the production process of LIB and LIB itself are not “green” [28]. Using cathode base on Fe element also bring other benefit. Because Fe is abundant in earth, LFP has moderately low cost and there are no resource limitations in compare to other cathode materials [29].

LFP has its own issue that need to be solved. The strong covalent oxygen bonds mentioned previously also lead to low ionic diffusivity and poor electronic conductivity [30]. This is due to the separation of the FeO_6 octahedra by PO_4 polyanions significantly

`

reduces the electronic conductivity [31]. And only 1-D migration of Li^+ is allowed inside the LFP crystal [32]. Efforts are made from three aspects to circumvent the low conductivity of LFP. Among the approaches developed, three methods are generally applied. (1) Reduce the particle size of LFP to increase the surface area, and so decrease the diffusion length of Li^+ and electrons [33]–[36]. (2) Apply a conductive layer on the surface of LFP. And among different materials applied, carbon layer is used by many research group because its cost effectivity, high conductivity, and non-toxic [37]–[41]. (3) Dope Fe with other elements, such as Co [42], Ni [43], Mn [44], Zn [45], V [46], or combination of several elements [47], [48].

The three approaches are commonly combined and applied simultaneously. It should be notice, similar to pervious discussion, doping with heavy metal like Co, Ni, and Mn, will offset the environmental and non-toxic advantage of LFP.

`

1.3 Solid state synthesis of LFP

Table 1.2 concludes the approaches developed to synthesis LFP. For large scale industrial applications, usually there are three aspects considered: (1) processing cost, (2) manufacturing difficulty, (3) quality of produced LFP [17]. Among them, processing cost is reflected by (a) setup and precursors cost, which is accounted as sunk cost, and (b) reaction time and energy consumption, which are accounted as prospective cost. Here, although reaction time is positive correlated to the energy consumption, time constrains are always need to be considered independently in industrial. Thus reaction time is listed separately in the table. Then as discussed in Chapter 1.2, LFP has an issue of low ionic conductivity and electron conductivity. The quality of LFP mentioned here is more about the control of particle size which significantly impact both conductivity [49].

`

Table 1.2. Comparation of different LiFePO4 synthesis approaches

Approaches	Solid state method	Sol-gel processing	Microwave processing	Hydrothermal reaction	Spray pyrolysis
Particle size (nm)	>300	50-150	40-50	>200	40-200
Setup and precursors cost	Lowest	High	High	Medium	High
Reaction time	Long	Long	Short	Long	Short
Energy consumption	High	Low	Low	High	Low
Manufacturing difficulty in large scale	Easy	Difficult	Difficult	Easy	Difficult

`

Solid state method usually produces LFP with size scale of micrometers [50]–[52]. In compare, approaches like microwave processing [53]–[56], sol-gel processing [57]–[60], and spray pyrolysis [61]–[64] can produce LFP with size scale of nanometers. Especially for microwave processing, particles with 40 to 50 nm can be synthesized in a few seconds of time. Microwave processing can be regarded as a unique solid state approach which triggers reaction with microwave assisting. However, applying microwave also lead to a disadvantage of high cost. More importantly, the manufacturing difficulty of this approach is too high and not predictable. There is a challenge on controlling the output power of microwave. Also, the equipment, which can produce high enough power microwave to synthesis LFP in large scale, is difficult to setup [65]. Sol-gel processing, spray pyrolysis, or even hydrothermal reaction [66]–[69], also has a cost issue in compare to solid state method either because of complex equipment setup, expensive metal based precursors, or complex synthesis procedures.

Although LFP with smaller particle size can have a higher ionic conductivity and electron conductivity, it should be noticed that smaller particle also leads to a large surface area of LFP. The large surface area could facilitate side reactions with electrolytes, consume more lithium in forming the solid electrolyte interface (SEI) that consequently leads to a low capacity retention [70]. In addition, particles with larger surface area generally have low tap density. This usually results with low energy density for LIB. On the other hand, the improvement on LIB's rate performance, which is contributed by smaller particle size, shows less significant when charging and discharging rate is lower than 10 C [36]. So now

`

considered with the lower energy cost for manufacture again, micro size LFP synthesized via solid state approach is more preferred by industry when is about high-energy applications, where the energy density, battery mass and energy cost are more important than the high-rate capacity.

In general, solid state approach can be regarded as a calcination process of a mixture of iron (Fe(II)) salt, lithium compound and a phosphate source [71], [72]. The calcination temperature is varied from 400 to 800 ℃ and the calcination time is usually in 10 to 24 hours. Conventional solid state synthesis of LFP also requires inert gas (nitrogen or argon) or reductive atmosphere (adding additional hydrogen) to protect Fe(II) from oxidation.

The calcination mechanisms can be concluded in six different ways which are demonstrated in Figure 1.5 [73]. These mechanisms can be divided into five diffusion mechanisms: (1) surface diffusion from surface, (2) volume diffusion from surface, (3) boundary diffusion from boundary, (4) volume diffusion from boundary, (5) volume diffusion from dislocation, and one evaporation condensation mechanism.

`

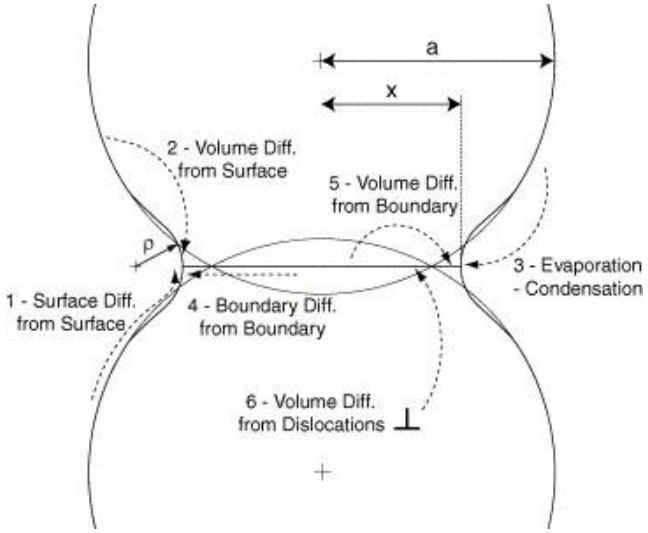

Figure 1.5. The six different sintering mechanisms

For the five mechanisms base on solid diffusion, the diffusion coefficient at different temperature is generally defined by Arrhenius equation [73]:

$$D = D_0 \bullet \exp(-\frac{E_A}{RT}) \qquad \text{Equation 1.1}$$

Where D is diffusion coefficient in m^2/s, D_0 is the diffusion coefficient when the temperature goes to infinity in m^2/s, E_A is the activation energy for diffusion in J/mol, R is universal gas constant which is 8.314 J/(mol K), T is the temperature in K. Calcination usually requires a higher reaction temperature and longer reaction time in compare to other synthesis approaches. This is because the diffusion coefficient for solid-solid reaction is usually low, and it lead to a low reaction rate.

A method to overcome this is to include mechanochemical activation in the process [74]–[76]. A heated ball-mill is usually applied in this case. Firstly, ball-mill offer precursors powder a kinetic energy which transfer to heat when collision between powders occurs.

`

The heat is then utilized to do the work and increase the temperature of precursors and consequently increases the diffusion coefficient and reaction rate. Secondly, mechanical activation of a mixture involves continuous renewal of contact surfaces. This results in pulverization, intimate powder mixing, and then solid-state reaction to a new phase. Instead of Fe (II) based iron source, a cheaper Fe (III) based iron source, such as Fe_2O_3 [76] or $FePO_4$ [77]is able to applied to decrease the total manufacture cost of LFP. Here, a carbon based material will be applied as a reduce agent for Fe (III). In this case, carbonized LFP can be directly synthesized. No further carbonization step is required to improve the ionic and electron conductivity of LFP.

`

Reference:

[1] M. Park, J. Kim, Y. Kim, N. Choi, and J. Kim, “R ev i e w Recent Advances in Rechargeable Magnesium Battery Technology : A Review of the Field s Current Status and Prospects R ev i e w,” vol. 714, pp. 570–585, 2015.

[2] N. Nitta, F. Wu, J. T. Lee, and G. Yushin, “Li-ion battery materials : present and future,” *Biochem. Pharmacol.*, vol. 18, no. 5, pp. 252–264, 2015.

[3] W. Cesar, M. De Oliveira, G. Dias, A. Barbosa, L. Rodrigues, and D. Lemos, “Green selective recovery of lanthanum from Ni-MH battery leachate using aqueous two-phase systems,” *Chem. Eng. J.*, vol. 322, pp. 346–352, 2017.

[4] J. E. Carrasco and D. Serrano-jim, “A Ni e Cd battery model considering state of charge and hysteresis effects,” vol. 275, 2015.

[5] P. T. Moseley, D. A. J. Rand, and K. Peters, “Enhancing the performance of lead e acid batteries with carbon e In pursuit of an understanding,” *J. Power Sources*, vol. 295, pp. 268–274, 2015.

[6] N. Alias and A. A. Mohamad, “Advances of aqueous rechargeable lithium-ion battery : A review,” *J. Power Sources*, vol. 274, pp. 237–251, 2015.

[7] K. Ozawa, *Lithium Ion Rechargeable Batteries: Materials, Technology, and New Applications*. 2012.

[8] C. Daniel *et al.*, “Cathode materials review Cathode Materials Review,” vol. 26, no. February, 2015.

[9] V. Gariépy *et al.*, “Effect of the Carbonization on the LiFePO4 Particles of Positive Electrode for Rechargeable Lithium Batteries,” *ECS Trans.*, vol. 58, no. 14, pp. 73–78, 2014.

[10] M. Naumann, R. C. Karl, C. N. Truong, A. Jossen, and H. C. Hesse, “Lithium-ion battery cost analysis in PV-household application,” *Energy Procedia*, vol. 73, pp. 37–47, 2015.

[11] D. Doughty and E. P. Roth, “A General Discussion of Li Ion Battery Safety,” *Electrochem. Soc. Interface*, pp. 37–44, 2012.

[12] M. M. Doeff, *Battery Cathodes*. 2013.

[13] D. Jugovi, N. Cvjeti, D. Uskokovi, F. R. Vukajlovi, and A. S. Milo, “Crystal structure analysis and first principle investigation of F doping in LiFePO 4,” *J. Power Sources*, vol. 241, pp. 70–79, 2013.

[14] J. Li, W. Yao, S. Martin, and D. Vaknin, “Lithium ion conductivity in single crystal LiFePO4,” *Solid State Ionics,* vol. 179, no. 2008, pp. 2016–2019, 2008.

[15] A. S. Andersson and J. O. Thomas, “The source of first-cycle capacity loss in LiFePO4,” *J. Power Sources*, vol. 98, pp. 498–502, 2001.

`

[16] C. Daniel *et al.*, “Cathode materials review Cathode Materials Review,” *AIP Conf. Proc.*, vol. 26, no. 1597, 2014.

[17] W. Zhang, “Structure and performance of LiFePO4 cathode materials : A review,” *J. Power Sources*, vol. 196, no. 6, pp. 2962–2970, 2011.

[18] B. Ellis, L. K. Perry, D. H. Ryan, and L. F. Nazar, “Small Polaron Hopping in Li x FePO4 Solid Solutions : Coupled Lithium-Ion and Electron Mobility,” *J. Am. Chem. Soc*, vol. 128, no. 35, pp. 11416–11422, 2006.

[19] R. Amin, J. Maier, P. Balaya, D. P. Chen, and C. T. Lin, “Ionic and electronic transport in single crystalline LiFePO4 grown by optical floating zone technique,” *Solid State Ionics*, vol. 179, pp. 1683–1687, 2008.

[20] V. Srinivasan and J. Newman, “Discharge Model for the Lithium Iron-Phosphate Electrode,” *J. Electrochem. Soc.*, vol. 151, no. 10, pp. 1517–1529, 2004.

[21] C. Delmas, M. Maccario, L. Croguennec, F. Le Cras, and F. Weill, “Lithium deintercalation in LiFePO4 nanoparticles via a domino-cascade model,” *Nat. Mater.*, vol. 7, pp. 665–671, 2008.

[22] G. K. Singh, G. Ceder, and M. Z. Bazant, “Intercalation dynamics in rechargeable battery materials : General theory and phase-transformation waves in LiFePO 4,” *Electrochim. Acta*, vol. 53, no. 26, pp. 7599–7613, 2008.

[23] M. Takahashi, S. Tobishima, K. Takei, and Y. Sakurai, “Reaction behavior of LiFePO 4 as a cathode material for rechargeable lithium batteries,” *Solid State Ionics*, vol. 148, no. 3–4, pp. 283–289, 2002.

[24] C. Vogler, G. Arnold, J. Garche, R. Hemmer, and S. Stro, “Fine-particle lithium iron phosphate LiFePO4 synthesized by a new low-cost aqueous precipitation technique,” *J. Power Sources*, vol. 119–121, pp. 247–251, 2003.

[25] J. R. Dahn and E. W. Fuller, “NmCS Thermal stability of LixCoO2 , LixNiO2 and 2-MnO2 and consequences for the safety of Li-ion cells,” *Solid State Ionics*, vol. 69, pp. 265–270, 1994.

[26] J. Lee, P. Kumar, J. Lee, B. M. Moudgil, and R. K. Singh, “ZnO incorporated LiFePO4 for high rate electrochemical performance in lithium ion rechargeable batteries,” *J. Alloys Compd.*, vol. 550, pp. 536–544, 2013.

[27] J. Wang *et al.*, “Cycle-life model for graphite-LiFePO4 cells,” *J. Power Sources*, vol. 196, no. 8, pp. 3942–3948, 2011.

[28] B. X. Wu, L. Jiang, F. Cao, Y. Guo, and L. Wan, “LiFePO4 Nanoparticles Embedded in a Nanoporous Carbon Matrix : Superior Cathode Material for Electrochemical Energy-Storage Devices,” *Adv. Mater.*, vol. 21, pp. 2710–2714, 2009.

`

[29] K. Striebel *et al.*, “The development of low cost LiFePO 4 -based high power lithium-ion batteries,” *J. Power Sources*, vol. 146, no. 1–2, pp. 33–38, 2005.

[30] X. Tang, L. Li, Q. Lai, X. Song, and L. Jiang, “Investigation on diffusion behavior of Li + in LiFePO 4 by capacity intermittent titration technique (CITT),” *Electrochem. Acta*, vol. 54, pp. 2329–2334, 2009.

[31] Y. Chiang, “lithium storage electrodes,” vol. 1, no. October, pp. 123–128, 2002.

[32] Morgan, D., A. Van der Ven, and G. Ceder, “Li Conductivity in LixMPO4 (M = Mn, Fe, Co, Ni) Olivine Materials,” *Electrochem. Solid-State Lett.*, vol. 7, no. 2, pp. A30–A32, 2004.

[33] J. Wu, G. Krishna, P. Dathar, and C. Sun, “In situ Raman spectroscopy of LiFePO4 : size and morphology dependence during charge and self-discharge,” *Nanotechnology*, vol. 24, 2013.

[34] C. Lifepo *et al.*, “Influence of Particle Size and Crystal Orientation on the Electrochemical Behavior of LiFePO4,” *J. Phys. Chem.*, vol. 114, no. 29, pp. 12598–12603, 2010.

[35] C. Delacourt, P. Poizot, S. Levasseur, and C. Masquelier, “Size Effects on Carbon-Free LiFePO 4 Powders The Key to Superior Energy Density,” *Electrochem. Solid-State Lett.*, vol. 9, no. 7, pp. 352–355, 2006.

[36] M. Gaberscek, R. Dominko, and J. Jamnik, “Is small particle size more important than carbon coating ? An example study on LiFePO4 cathodes,” *Electrochem. commun.*, vol. 9, no. 12, pp. 2778–2783, 2007.

[37] X. Zhi, G. Liang, L. Wang, X. Ou, L. Gao, and X. Jie, “Optimization of carbon coatings on LiFePO 4 : Carbonization temperature and carbon content,” *J. Alloys Compd.*, vol. 503, no. 2, pp. 370–374, 2010.

[38] O. Toprakci, L. Ji, Z. Lin, H. A. K. Toprakci, and X. Zhang, “Fabrication and electrochemical characteristics of electrospun LiFePO 4 / carbon composite fibers for lithium-ion batteries,” *J. Power Sources*, vol. 196, no. 18, pp. 7692–7699, 2011.

[39] W. Wei, W. Lv, M. Wu, F. Su, Y. He, and B. Li, “The effect of graphene wrapping on the performance of LiFePO 4 for a lithium ion battery,” *Carbon N. Y.*, vol. 57, pp. 530–533, 2013.

[40] S. Sun *et al.*, “Microporous and Mesoporous Materials One-pot synthesis of LiFePO 4 – carbon mesoporous composites for Li-ion batteries,” *MICROPOROUS MESOPOROUS Mater.*, vol. 198, pp. 175–184, 2014.

[41] C. Zhang, Y. Liang, L. Yao, and Y. Qiu, “Effect of thermal treatment on the properties of electrospun LiFePO 4 – carbon nanofiber composite cathode materials for lithium-ion batteries,” *J. Alloys Compd.*, vol. 627, pp. 91–100, 2015.

`

[42] H. Gao, L. Jiao, J. Yang, Z. Qi, Y. Wang, and H. Yuan, "High rate capability of Co-doped LiFePO 4 / C," *Electrochim. Acta*, vol. 97, pp. 143–149, 2013.

[43] Y. Ge, X. Yan, J. Liu, X. Zhang, and J. Wang, "An optimized Ni doped LiFePO 4 / C nanocomposite with excellent rate performance," *Electrochim. Acta*, vol. 55, no. 20, pp. 5886–5890, 2010.

[44] C. Li, N. Hua, C. Wang, and X. Kang, "Effect of Mn 2 + -doping in LiFePO 4 and the low temperature electrochemical performances," *J. Alloys Compd.*, vol. 509, no. 5, pp. 1897–1900, 2011.

[45] H. Liu, Q. Cao, L. J. Fu, C. Li, Y. P. Wu, and H. Q. Wu, "Doping effects of zinc on LiFePO 4 cathode material for lithium ion batteries," *Electrochem. commun.*, vol. 8, no. 10, pp. 1553–1557, 2006.

[46] C. S. Sun *et al.*, "Improved high-rate charge / discharge performances of LiFePO 4 / C via V-doping," *J. Power Sources*, vol. 193, no. 2, pp. 841–845, 2009.

[47] H. Shu *et al.*, "Improved electrochemical performance of LiFePO 4 / C cathode via Ni and Mn co-doping for lithium-ion batteries," *J. Power Sources*, vol. 237, pp. 149–155, 2013.

[48] D. Wang, H. Li, S. Shi, X. Huang, and L. Chen, "Improving the rate performance of LiFePO 4 by Fe-site doping," *Electrochim. Acta*, vol. 50, no. 14, pp. 2955–2958, 2005.

[49] Y. Chang and C. Peng, "Effects of particle size and carbon coating on electrochemical properties of LiFePO 4 / C prepared by hydrothermal method," *J. Mater. Sci.*, vol. 49, no. 20, pp. 6907–6916, 2014.

[50] F. Cheng *et al.*, "High power performance of nano-LiFePO4/C cathode material synthesized via lauric acid-assisted solid-state reaction," *Electrochim. Acta*, vol. 56, no. 8, pp. 2999–3005, 2011.

[51] K. Konstantinov *et al.*, "New approach for synthesis of carbon-mixed LiFePO4 cathode materials," *Electrochim. Acta*, vol. 50, pp. 421–426, 2004.

[52] C. H. Mi, G. S. Cao, and X. B. Zhao, "Low-cost , one-step process for synthesis of carbon-coated LiFePO4 cathode," *Electrochim. Acta*, vol. 59, pp. 127–130, 2005.

[53] Z. Guo and Z. Chen, "Preparation of LiFePO 4 / Graphene Composites by Microwave-Assisted Solvothermal Method 1," *Russ. J. Appl. Chem.*, vol. 89, no. 12, pp. 2072–2075, 2016.

[54] Y. Meng, Z. Zhang, W. Han, and Y. Zhang, "Synthesis of Carbon-Coated LiFePO 4 Cathode Material by One-Step Microwave-Assisted Pyrolysis of Ionic Liquid Process," *Nano*, vol. 11, no. 1, pp. 1–7, 2016.

[55] J. Lim *et al.*, "Direct formation of LiFePO 4 / graphene composite via microwave-

assisted polyol process," *J. Power Sources*, vol. 304, pp. 354–359, 2016.

[56] B. Han, X. Meng, L. Ma, and J. Nan, "Nitrogen-doped carbon decorated LiFePO 4 composite synthesized via a microwave heating route using polydopamine as carbon – nitrogen precursor," *Ceram. Int.*, vol. 42, no. 2, pp. 2789–2797, 2016.

[57] Y. Hu, M. M. Doeff, R. Kostecki, and R. Finones, "Electrochemical Performance of Sol-Gel Synthesized LiFePO 4 in Lithium Batteries," *J. Electrochem. Soc.*, vol. 151, no. 8, pp. 4–10, 2004.

[58] D. Choi and P. N. Kumta, "Surfactant based sol – gel approach to nanostructured LiFePO 4 for high rate Li-ion batteries," *J. Power Sources*, vol. 163, no. 2, pp. 1064–1069, 2007.

[59] M. A. E. Sanchez, G. E. S. Brito, M. C. A. Fantini, G. F. Goya, and J. R. Matos, "Synthesis and characterization of LiFePO 4 prepared by sol – gel technique," *Solid State Ionics*, vol. 177, no. 5–6, pp. 497–500, 2006.

[60] D. A. Ziolkowska, J. B. Jasinski, K. P. Bartosz, Hamankiewicz Korona, S. Wu, and A. Czerwinski, "In Situ XRD and TEM Studies of Sol-Gel-Based Synthesis of LiFePO4," *Cryst. Growth Des.*, vol. 16, no. 9, pp. 5006–5013, 2016.

[61] R. Kashi, M. Khosravi, and M. Mollazadeh, "Effect of carbon precursor on electrochemical performance of LiFePO4 - C nano composite synthesized by ultrasonic spray pyrolysis as cathode active material for Li ion battery," *Mater. Chem. Phys.*, vol. 203, pp. 319–332, 2018.

[62] M. Yang, T. Teng, and S. Wu, "LiFePO4 / carbon cathode materials prepared by ultrasonic spray pyrolysis," *J. Power Sources*, vol. 159, no. 13, pp. 307–311, 2006.

[63] M. Konarova and I. Taniguchi, "Preparation of LiFePO4/C composite powders by ultrasonic spray pyrolysis followed by heat treatment and their electrochemical properties," *Mater. Res. Bull.*, vol. 43, no. 12, pp. 3305–3317, 2008.

[64] S. H. Ju and Y. C. Kang, "LiFePO4/C cathode powders prepared by spray pyrolysis from the colloidal spray solution containing nano-sized carbon black," *Mater. Chem. Phys.*, vol. 107, no. 2–3, pp. 328–333, 2008.

[65] C. Gao, J. Zhou, G. Liu, and L. Wang, "Applied Surface Science Lithium-ions diffusion kinetic in LiFePO 4 / carbon nanoparticles synthesized by microwave plasma chemical vapor deposition for lithium-ion batteries," *Appl. Surf. Sci.*, vol. 433, pp. 35–44, 2018.

[66] S. Bolloju *et al.*, "A green and facile approach for hydrothermal synthesis of LiFePO 4 using iron metal directly," *Electrochim. Acta*, vol. 220, pp. 164–168, 2016.

[67] H. Yen, R. Rohan, C. Chiou, C. Hsieh, and S. Bolloju, "Hierarchy concomitant in situ stable iron (II) À carbon source manipulation using ferrocenecarboxylic acid

for hydrothermal synthesis of LiFePO 4 as high-capacity battery cathode," *Electrochim. Acta*, vol. 253, pp. 227–238, 2017.

[68] S. Tajimi, Y. Ikeda, K. Uematsu, K. Toda, and M. Sato, "Enhanced electrochemical performance of LiFePO 4 prepared by hydrothermal reaction," *Solid State Ionics*, vol. 175, no. 1–4, pp. 287–290, 2004.

[69] B. Jin and H. Gu, "Preparation and characterization of LiFePO 4 cathode materials by hydrothermal method," *Solid State Ionics*, vol. 178, no. 37–38, pp. 1907–1914, 2008.

[70] D. Li, D. Danilov, Z. Zhang, H. Chen, and Y. Yang, "Modeling the SEI-Formation on Graphite Electrodes in LiFePO4 Batteries," *J. Electrochem. Soc.*, vol. 162, no. 6, pp. 858–869, 2015.

[71] J. Zheng, X. Li, Z. Wang, H. Guo, and S. Zhou, "LiFePO4 with enhanced performance synthesized by a novel synthetic route," *J. Power Sources*, vol. 184, pp. 574–577, 2008.

[72] Z. Chen, H. Zhu, S. Ji, R. Fakir, and V. Linkov, "Influence of carbon sources on electrochemical performances of LiFePO 4 / C composites," *Solid State Ionics*, vol. 179, pp. 1810–1815, 2008.

[73] M. F. Ashby, "A first report x on sintering diagram," *Acta Met.*, vol. 22, no. 3, pp. 275–289, 1974.

[74] J. Kim, G. Cheruvally, J. Ahn, G. Hwang, and J. Choi, "Electrochemical properties of carbon-coated LiFePO4 synthesized by a modified mechanical activation process," *J. Phys. Chem. Solids*, vol. 69, pp. 2371–2377, 2008.

[75] H. Chul, W. Il, and H. Jang, "Electrochemical properties of carbon-coated LiFePO4 cathode using graphite , carbon black , and acetylene black," *Electrochim. Acta*, vol. 52, pp. 1472–1476, 2006.

[76] C. Woo, M. Hee, W. Tae, and K. Sub, "Synthesis of olivine LiFePO 4 cathode materials by mechanical alloying using iron (III) raw material," *J. Power Sources*, vol. 146, pp. 534–538, 2005.

[77] B. Q. Zhu, X. H. Li, Z. X. Wang, and H. J. Guo, "Novel synthesis of LiFePO 4 by aqueous precipitation and carbothermal reduction," *Mater. Chem. Phys.*, vol. 98, pp. 373–376, 2006.

`

Chapter 2 The Crystal Structure Engineering on Synthesis of $LiFePO_4$ via Lithiation under un Unrestricted Environment

2.1 Introduction

LIBs have been applied in many areas such as electric vehicle, portable electronic devices, and large scale energy storage system[1]. In compare to other rechargeable batteries such as lead–acid battery or alkaline battery, LIBs have higher working voltage, higher specific energy, and longer cycle life [2]. Among different cathode materials, LFP has been widely used as a commercial cathode material in LIBs because of its cost efficiency, environment friendliness, and magnificent thermal stability [3]. Currently many methods have been developed to synthesize LFP, such as sol-gel [4], microwave-assisted synthesis [5], hydrothermal [6], spray pyrolysis [7], solid state reaction [8], and approaches base on combination of these methods [9]. However, solid state method is still the only approach which can be commercialized mainly due to its cost-effective processing [3].

The traditional solid state reaction has disadvantages on its synthesis process such as inert gas environment, long reaction time up to 10 hours, and high reaction temperature around 700 °C [10]–[12]. Our approach is to overcome those disadvantages by applying lithium acetate as lithium source, so that the low-temperature and short-reaction time under an unrestricted environment synthesis process is developed. However, the existence of oxygen in the unrestricted environment syhthesis, leads to the yield of byproduct that will decrease the quality of synthesized LFP [13]. These byproducts are mainly iron oxide in different crystal structure, such as α-Fe_2O_3 and γ-Fe_2O_3 and lithium phosphate. Recent works showed that the crystal structure of $FePO_4$ has significant influence on produced LFP in

`

solid state method [14]. Anhydrous $FePO_4$, which is acquired by a dehydration process of commercially available $FePO_4$ hydrates, can exist in different forms. Depending on the phase transition temperature and pressure, anhydrous $FePO_4$ can exist in $CrVO_4$ structure, monoclinic phosphosiderite, trigonal α-quartz or a mixed state of these forms [15]. Beside these three structures, $FePO_4$ can also exist in olivine structure which is the delithiated form of $LiFePO_4$. The schematic diagrams for these four crystal structure are demonstrated in Figure 2.1[16]. $FePO_4$ with olivine structure has a space group of Pnma. It is stable but usually only exist in LIB based LFP cathode, and it will transfer to quartz structure at high temperature. On the other side, $FePO_4$ with $CrVO_4$ structure has a space group of Cmcm. It is usually acquired under high pressure synthesis. Both structures have Fe sites coordinated by six nearest-neighbor O atoms in approximately octahedral geometry. In the case of monoclinic structure ($P2_1/n$), the Fe sites have lower symmetry and their coordination with nearest neighbor O atoms is approximately 5. $FePO_4$ with monoclinic structure is in metastable state. It will also transfer to the quartz $FePO_4$ with heating as driving force. Therefore, quartz structure ($P3_121$) is the most stable form for dehydrated $FePO_4$ which is used in LFP synthesis. Quartz $FePO_4$ has Fe sites coordinated by four nearest neighbor O atoms in approximately tetrahedral geometry.

(a) olivine structure

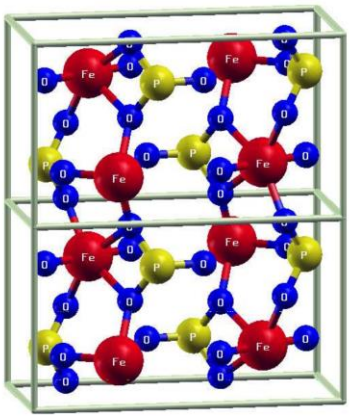

(b) $CrVO_4$ structure

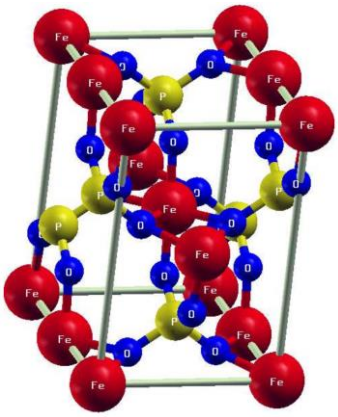

(c) trigonal α-quartz structure

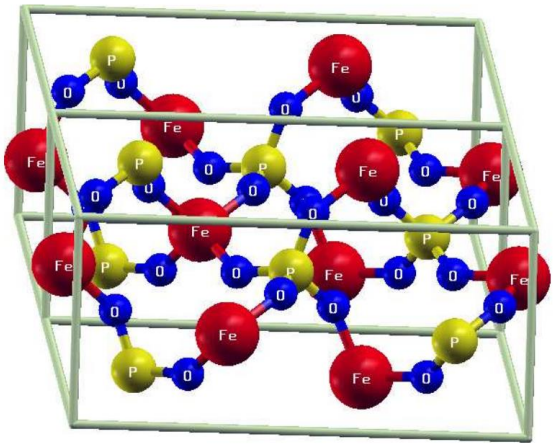

(d) monoclinic structure

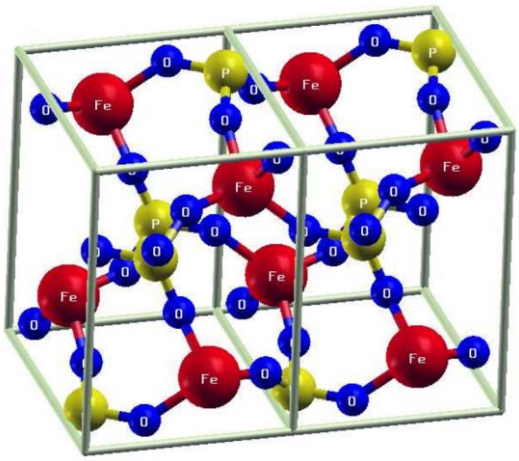

Figure 2.1. The crystal structure for (a) olivine (b) $CrVO_4$ (c) trigonal α-quartz and (d) monoclinic $FePO_4$

`

Furthermore, phase transition temperature has impact on morphology, particle size and its distribution, of anhydrous $FePO_4$. Both crystal structure and morphology of $FePO_4$ significantly influence the growth of LFP and its particle size in the following solid state reaction [14]. Since lithiation is also based on carbon thermal solid-state reaction, and $FePO_4$ is frequently used as iron source in solid-state reaction method, the form of $FePO_4$ will also play an important role in lithiation in an unrestricted environment approach. In this dissertation, a lithiation of iron phosphate is applied to synthesize LFP via heating the mixture of precursors in an unrestricted environment. $FePO_4$ with different forms are used to synthesize LFP under an unrestricted environment to study the influence of dehydration process of $FePO_4 \cdot 2H_2O$ in the LFP synthesis. The crystallinity, morphology, and thermal characteristics of synthesized LFP are studied to examine the feasibility to synthesis crystalline LFP via lithiation in an unrestricted environment approach.

2.2 Experiment procedure

$FePO_4 \cdot 2H_2O$ (Sigma-Aldrich) was dehydrated in a muffle furnace at two different temperatures (300 and 600 ℃) for 4 hours with 10 ℃/min ramping rate. Anhydrous $FePO_4$ powders were taken out from furnace after it was cooled to room temperature. The $FePO_4$ was then mixed with lithium acetate in stoichiometric by a vertex mixer for 1 hour. The mixture was placed in a lime glass tubular reaction vessel with one terminal end. The dimension of container is 10 cm in length, 3 mm in radius and the intake of it was 0.5 mm in radius. The 0.6 g of precursors were loaded in each container. Two containers were placed into a mullite round single bore tubes (one end closed) in each synthesis process.

`

This container was applied due to the necessity of air flow controlling during heating process to limited the oxidation rate and improve the quality of yield LFP. The mullite tube was inserted into a muffle furnace once it reached to the reaction temperature, 540 ℃ and maintained for 21 mins. The tube was pulled out once the reaction finished and then cooled down to the room temperature.

X-ray diffraction (XRD) was applied to analyze the crystalline phase of synthesized anhydrous $FePO_4$ and LFP. Differential scanning calorimetry (DSC) and thermogravimetric analysis (TGA) were performed to study the dehydration and phase transition behavior for $FePO_4$ and lithium acetate. The particle size and morphology were observed via a scanning electron microscopy (SEM).

2.3 Results and discussion

The dehydration process of $FePO_4 \cdot 2H_2O$ was firstly studied by TGA. $FePO_4 \cdot 2H_2O$ contains 19.27 wt% of water based on its chemical formula. The dehydration process was conducted by TGA with heating rate of 20 ℃/min to 300 and 600 ℃ and maintained for 6 hours, respectively. The TGA result in wt% vs time plot was obtained as shown in Figure 2.2. $FePO_4$ dehydrated at 300 ℃ has a weight loss of 19.43%, while $FePO_4$ dehydrated at 600 ℃ has a weight loss of 20.26%. The excess part of weight loss represented burning of impurities [17]. With 0.83% less of remaining product, dehydration at 600 ℃ is able to eliminate impurities more efficiently. Both TGA curve reach stable status after 4 hours of heating because the weight change after 4 hours was less than 0.1%. Thus, 4 hours of heating time in $FePO_4 \cdot 2H_2O$ dehydration process was applied in the following experiment.

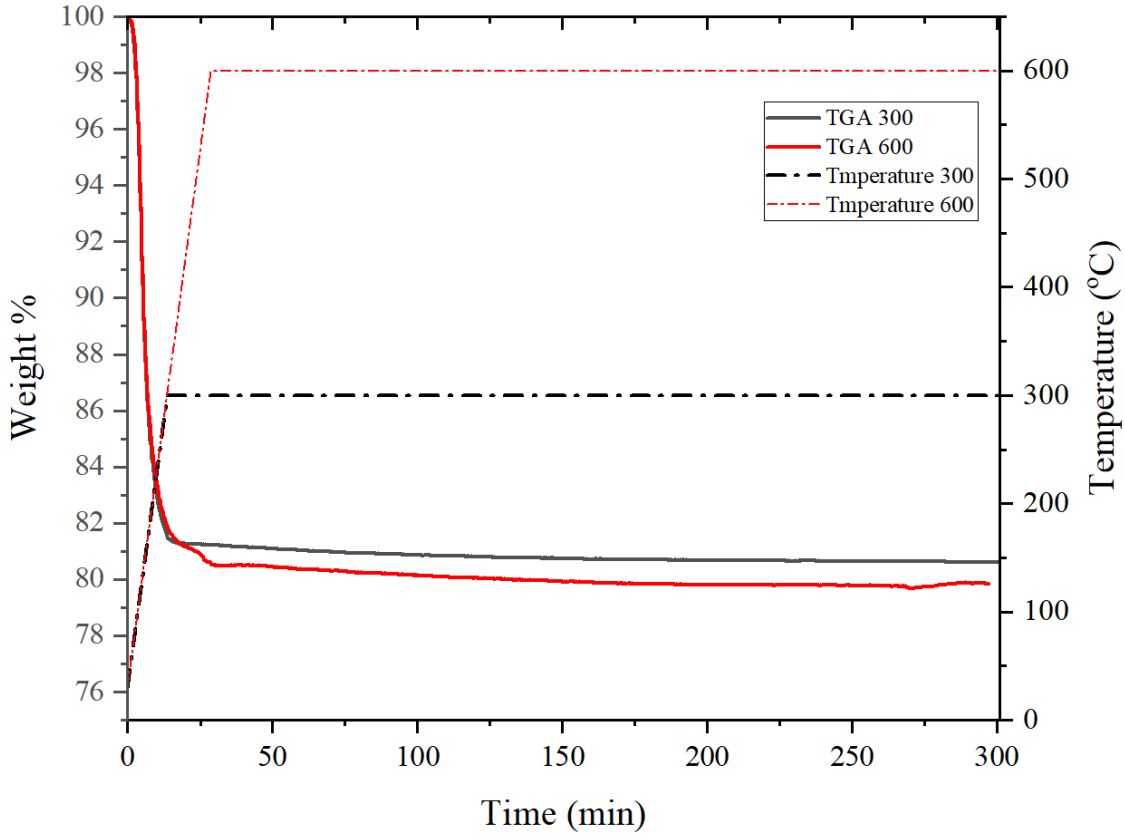

Figure 2.2. The results of TGA for $FePO_4$ dehydrated under 300 ℃ and 600 ℃

`

As shown in Figure 2.3, $FePO_4 \cdot 2H_2O$ has an amorphous structure because no characterization peaks are shown in the XRD pattern. Similar patterns are observed in $FePO_4$ dehydrated under 300 ℃, meaning the crystal structure of $FePO_4$ is still maintained as amorphous. In contrast, $FePO_4$ dehydrated under 600 ℃ has a significant change on XRD patterns which demonstrates the yielding of α-quartz $FePO_4$ with a trigonal structure. This crystal structure is characterized by the strongest diffraction peak of (012) shown at 26° and the second strongest diffraction peak of (100) at 21°. The XRD patterns demonstrated that a crystal phase transition is triggered at a temperature between 300 ℃ and 600 ℃. Above this temperature, amorphous $FePO_4$ is transferred to quartz $FePO_4$.

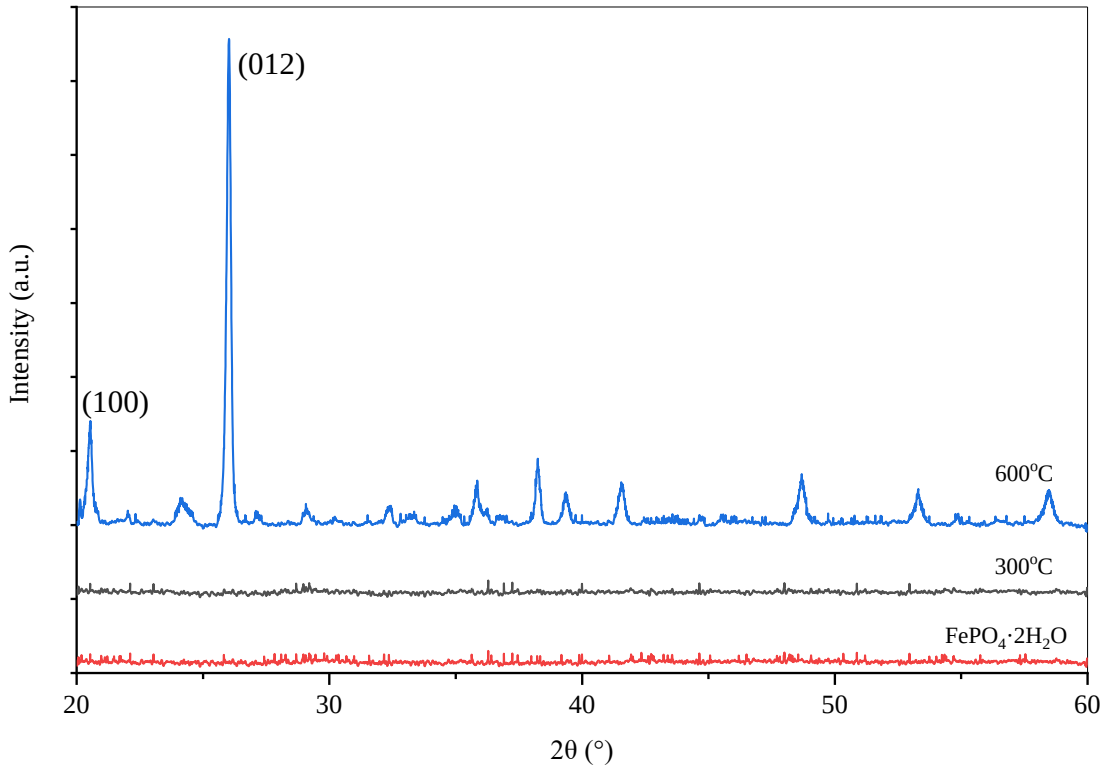

Figure 2.3. The XRD patterns for anhydrate $FePO_4$ and $FePO_4$ dehydrated under 300 ℃ and 600 ℃

`

The significant change of particle size distribution is observed by SEM. As demonstrated in Figure 2.4, $FePO_4$ dehydrated at 300 ℃ shows particles with a size around 100 nm. On the other hand, $FePO_4$ dehydrated at 600 ℃ shows very clear particles with size from 100 to 1000 nm. The crystal structures of commercially available $FePO_4 \cdot 2H_2O$ are vary depending on the vendor. In this case, the amorphous $FePO_4 \cdot 2H_2O$ lead to the amorphous $FePO_4$. However, with 4 hours of heating under 600 ℃, all materials transfer to a quartz structure as mentioned previously [18]. The phase transition causes the significant change on morphology. It results that quartz $FePO_4$ has larger particle size than amorphous $FePO_4$.

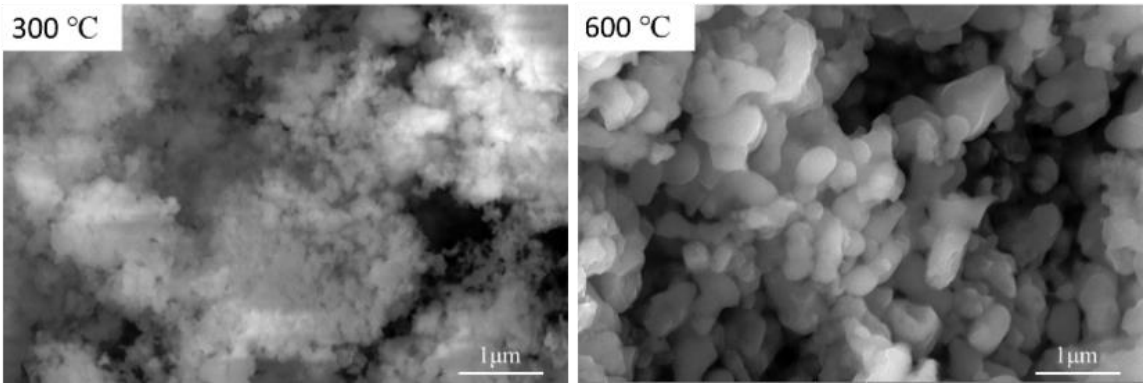

Figure 2.4. The results of SEM for $FePO_4$ dehydrated under 300 ℃ and 600 ℃

Since a crystal transition occurred below 600 ℃ and higher than 300 ℃, and the LFP synthesis temperature is 540 ℃, it is important to know if LFP synthesis temperature is higher or lower than $FePO_4$ phase transition temperature. Such an issue is investigated by DSC. Figure 2.5 is the DSC result of heating $FePO_4 \cdot 2H_2O$ from room temperature to 600 ℃ with a heating rate of 20 ℃/min. The DSC curve exhibited two peaks located at about 100 ℃ and 590 ℃, which corresponded to the endothermic peak of dehydration and crystal

`

transition process. The crystal transition is started around 590 ℃. Consider the reaction temperature applied is 540 ℃, no crystallization of amorphous $FePO_4$ is triggered in LFP300 synthesis. The low quality of LFP300 is mainly resulted by using amorphous $FePO_4$.

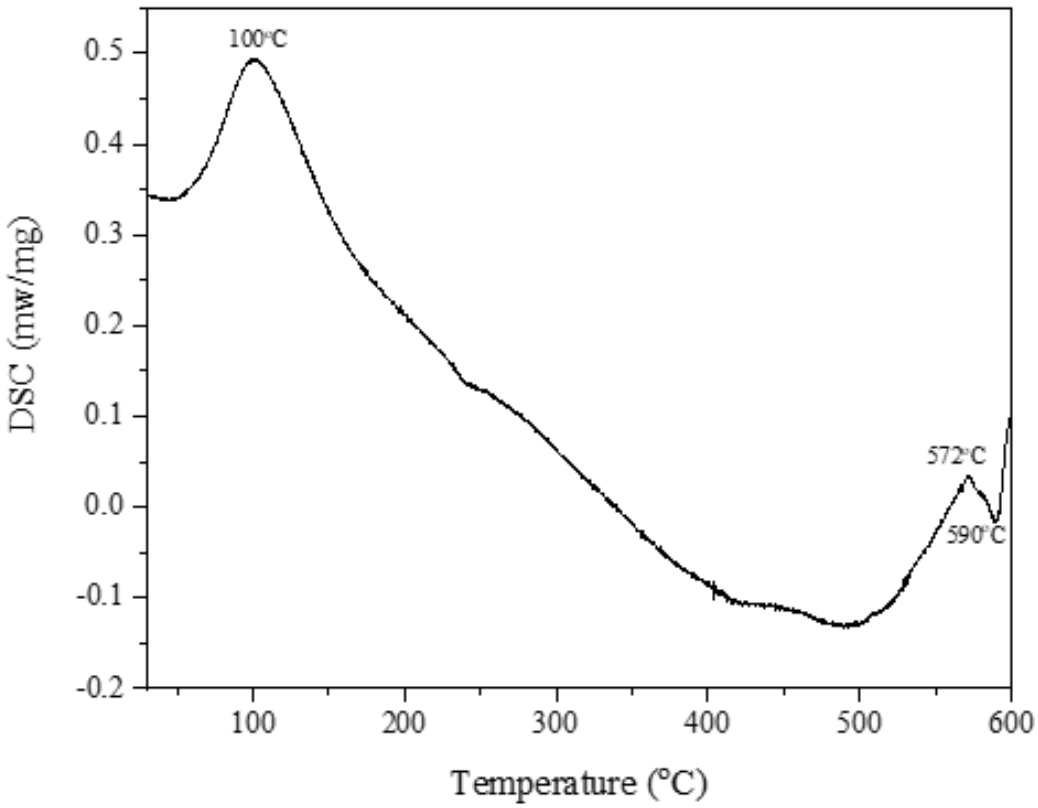

Figure 2.5. The DSC for heating $FePO_4 \cdot 2H_2O$ from room temperature to 600 °C.

`

The LFP was then synthesized with $FePO_4$ dehydrated at 300 ℃ and 600 ℃ (LFP300 and LFP600), respectively. XRD was applied to investigate the crystal structure of products. As demonstrated in Figure 2.6, when compare to the reference (XRD patterns of pristine LFP), it is clear that LFP300 has poor quality if LFP due to its strong α-Fe_2O_3 peak and γ-Fe_2O_3 peak. This means oxidation reaction becomes more significant which lead to the yielding of α-Fe_2O_3 and γ-Fe_2O_3. On the other hand, the smaller noise to signal ratio demonstrates that LFP600 has a great crystallinity. It is mainly characterized by position and intensity to noise ratio of (101), (111)/ (201), (211), and (311) peaks which show around 21°, 26°, 30° and 36°, respectively. α-Fe_2O_3 has the strongest peak of (110) at the same position of LFP's (311) peak. Therefore, when significant oxidation occurs, like what demonstrated in LFP300, a 100% peak at 36° is presented. Besides α-Fe_2O_3, the amount of γ-Fe_2O_3, characterized by (220), (400), and (511) peaks, is also significant. Here, comparing the intensity ratio of (211) LFP and (220) γ-Fe_2O_3 is the most intuitive way to evaluate the quality of synthesized LFP. In this case LFP300 have a nearly 1:1 ratio while LFP600 has a 5:1 ratio. This means LFP300 with smaller number on ratio has more serious γ-Fe_2O_3 impurity issue. α-Fe_2O_3 will transfer to γ-Fe_2O_3 at high temperature [20] and causes the yielding of metastable γ-Fe_2O_3. In addition, the oxidation of LFP lead to the presents of Li_3PO_4, which can be characterized by (110), (101), (011) peaks. The intensity of Li_3PO_4 peaks is positively correlated to the oxidation degree. The completed oxidation reaction that yield byproduct can be summarized as:

`

$$12LiFePO_4\ (s) + 3O_2\ (g) \rightarrow 4Li_3PO_4\ (s) + 8FePO_4\ (s) + 2Fe_2O_3\ (s)$$

Any optimization made to minimize the oxidation should be able to lead a XRD result with both Li_3PO_4 peak and iron oxide peak becomes less significant when compare to the peaks of itself.

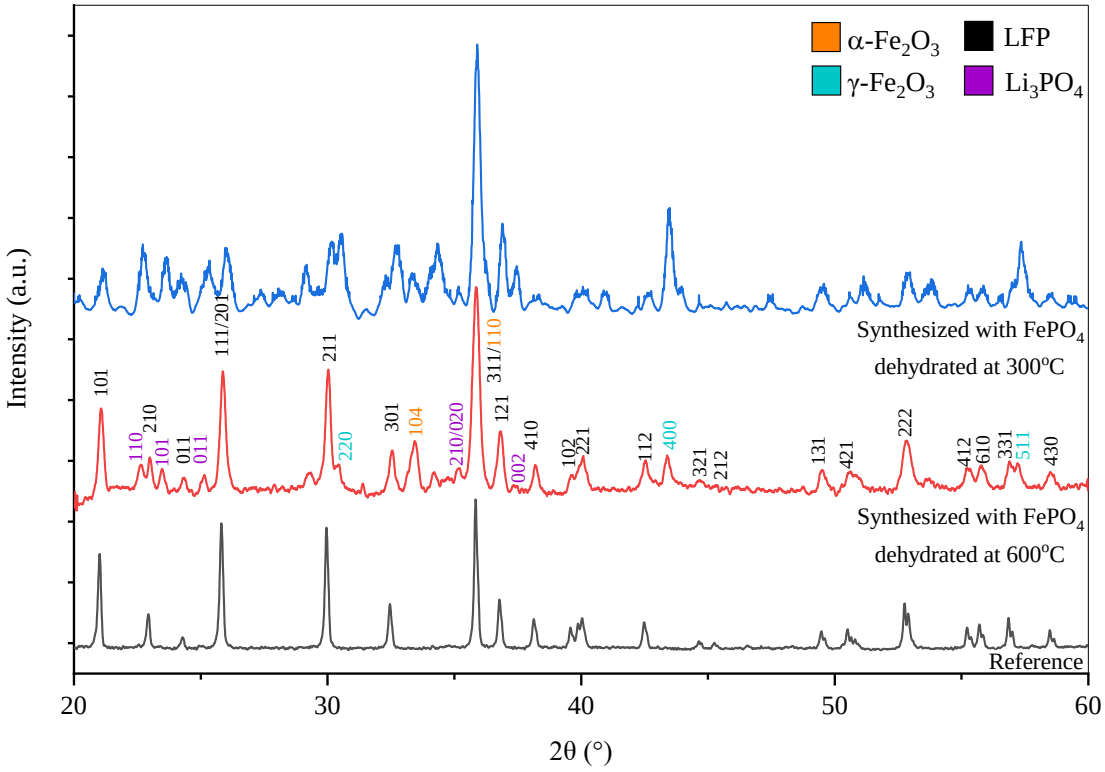

Figure 2.6. The XRD patterns, for LFP300 and LFP600

`

LFP300 and LFP600 were then characterized by SEM. LFP300 in Figure 2.7 has particle size from 500 to 1000 nm. However, since XRD patterns has shown a significant amount of impurities presented in its structure, it difficult to distinguish the LFP particles from other particles. LFP600 has particle size from 100 to 2000 nm. This wide size distribution is manly contributed by the wide size distribution of $FePO_4$ precursors.

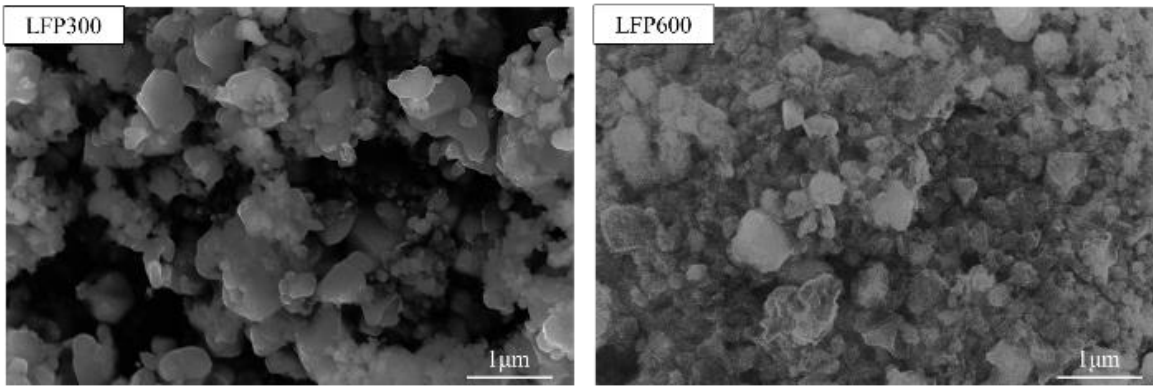

Figure 2.7. The SEM result for LFP300 and LFP600

As demonstrated above, the crystallinity of LFP synthesized via lithiation in an unrestricted environment is significantly impacted by the crystal structure of $FePO_4$. According to the result, using crystallized quartz $FePO_4$ lead to a better quality of LFP than using amorphous $FePO_4$. The solid state reaction between $FePO_4$ and lithium acetate can be concluded as Reaction 1:

$$4FePO_4(s) + 4CH_3COOLi\ (s) \rightarrow 4LiFePO_4\ (s) + 6H_2O\ (g) + CO_2\ (g) + 7C\ (s)$$

The rate of this reaction in compare to the oxidation significantly impact the quality of synthesized LFP. It has been introduced that five diffusion mechanisms are involved in

`

calcination [20]. However, without a crystalline structure, diffusion based on grain boundary and dislocation is limited. This results with the diffusion of amorphous material is mainly started on surface, which is (1) surface diffusion from surface, and (2) volume diffusion from surface. The barrier energy for amorphous surface is usually lower since it has less pack dense. Leading to a low activation energy for diffusion (E_A) of O_2 in Equation 1.1:

$$D = D_0 \bullet \exp(-\frac{E_A}{RT}) \qquad \text{Equation 1.1}$$

It can be concluded that the diffusion coefficient for O_2 is higher in this case. In addition, amorphous $FePO_4$ has larger porosity and less dense than quartz $FePO_4$, creates a larger contact area between oxygen and $FePO_4$ and so accelerates the oxidation process. Therefore, instead of LFP synthesis reaction, impact brought by the byproduct reaction (solid-gas oxidation reaction) becomes more significant. This is another reason low quality LFP is synthesized via amorphous $FePO_4$.

On the other hand, lithium acetate is also significantly impact the reaction of LFP synthesis. Figure 2.8 is the TGA and DSC result for heating DSC in air flow from room temperature to 600 ℃ with a heating rate of 20 ℃/min. It illustrates the decomposition process of lithium acetate: (1) the moisture is evaporated and lithium acetate is dehydrated at around 110 ℃. This lead to a weight loss of 6%; (2) lithium acetate is melted around 286 ℃ which related to the second peak in DSC and no weight change is observed in TGA; (3) lithium acetate started to decomposed at 400 ℃. This can be concluded as Reaction 2:

`

$$2CH_3COOLi\ (l) \rightarrow Li_2O\ (s) + 3H_2O\ (g) + 4C\ (s)$$

According to the stoichiometry of the reaction, the weight loss of this process is

$$Wt\% = \frac{3 \times N_{H_2O}}{2 \times N_{CH_3COOLi}} = 40.9\%$$

On the other hand, according to the TGA result, the decomposition process is started from 94% and ended at 53%. The weight loss in this case is:

$$Wt\% = \frac{94\% - 53\%}{94\%} = 43.6\%$$

Therefore, the TGA result is consisted with the decomposition reaction. The 2.7% error can be caused by the TGA system and the impurities contained in the lithium acetate.

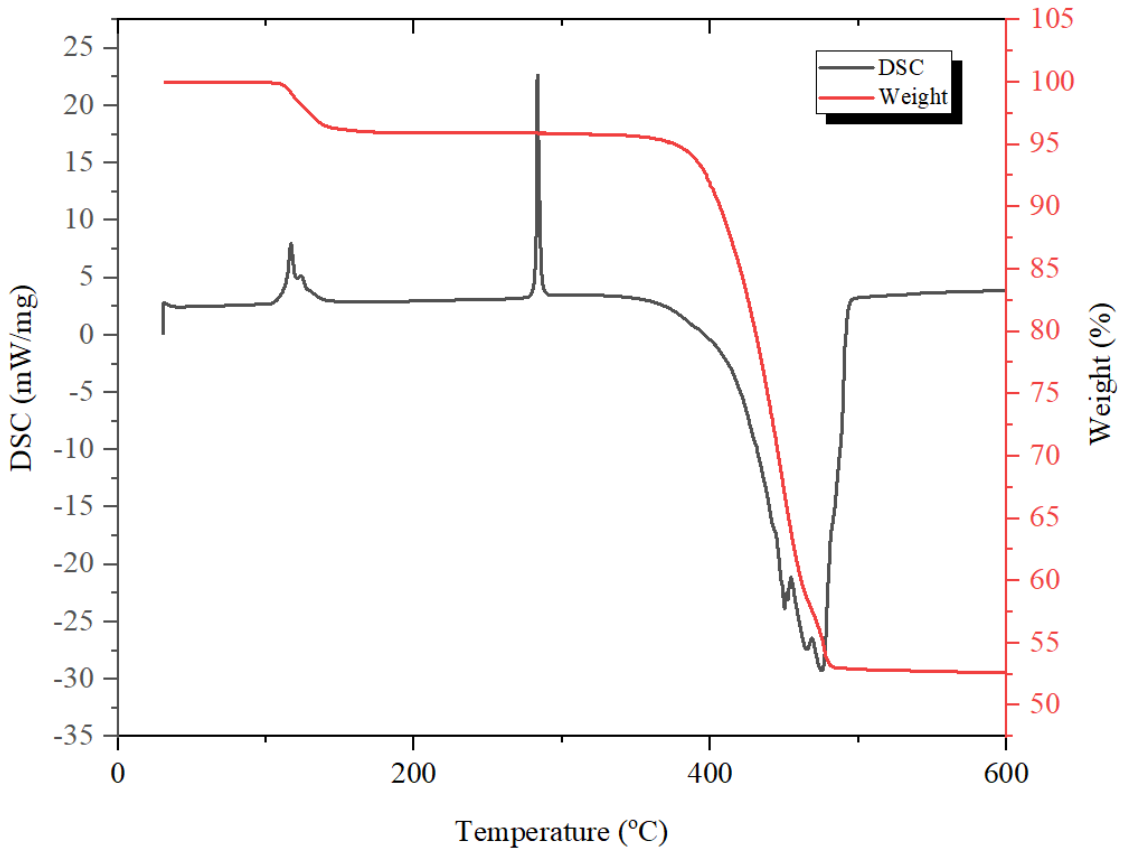

Figure 2.8. The TGA and DSC result for heating DSC in air flow from room temperature to 600 ℃ with a heating rate of 20 ℃/min

`

The synthesis of LFP can then be completed and denoted as Reaction 3:

$$4FePO_4\ (s) + 2Li_2O\ (s) + C\ (s) \rightarrow 4LiFePO_4\ (s) + CO_2\ (g)$$

The Reaction 1 mentioned at beginning is the combination of Reaction 2 and 3. Lithium acetate contains both lithium and carbon which makes the carbon thermal process can be completed with just two chemicals. Also, it should be noticed lithium acetate has a features that it melts before decompose (which is also before reacted with $FePO_4$). The liquid (lithium acetate)-solid ($FePO_4$) system improves the uniformity of precursors mixing which leads to a completed synthesis reaction (no $FePO_4$ observed in the XRD patterns of LFP600). It also increases the contact surface area between Li_2O, carbon that yielded via decomposition of lithium acetate and $FePO_4$, are increased. And it is possible that Li_2O and carbon is directly solidified on the surface of $FePO_4$ particles. The enhanced contact surface area then accelerates the diffusion rate and so increases the reaction rate. Therefore, LFP synthesized via this approached can be completed in 30 mins.

`

2.4 Conclusion

LFP was successfully synthesized via lithiation of dehydrated $FePO_4$ in an unrestricted environment. The crystal structure of dehydrated $FePO_4$ has significant impact on resulted LFP. Different crystal structures can be acquired by adjusting dehydration temperature of hydrated $FePO_4$. In this research, it is determined that LFP synthesized with quartz $FePO_4$ which dehydrated at 600 ℃ has better crystallinity and results LFP with higher quality in compare to LFP synthesized with amorphous $FePO_4$. Lithium acetate also plays a significant role in LFP synthesis. Its thermodynamics properties accelerate the LFP synthesis reaction that allow LFP to be produced in a relatively short time. The biggest challenge faced by the approach of lithiation in an unrestricted environment is the negative quality impact created by oxidation of LFP. Our special design of reaction tube successfully limits the air flow rate and so minimize the oxidation of LFP.

`

Reference:

[1] V. Etacheri, R. Marom, R. Elazari, G. Salitra, and D. Aurbach, "Challenges in the development of advanced Li-ion batteries: A review," *Energy Environ. Sci.*, vol. 4, no. 9, pp. 3243–3262, 2011.

[2] N. Nitta, F. Wu, J. T. Lee, and G. Yushin, "Li-ion battery materials: Present and future," *Mater. Today*, vol. 18, no. 5, pp. 252–264, 2015.

[3] T. V. S. L. Satyavani, A. Srinivas Kumar, and P. S. V. Subba Rao, "Methods of synthesis and performance improvement of lithium iron phosphate for high rate Li-ion batteries: A review," *Eng. Sci. Technol. an Int. J.*, vol. 19, no. 1, pp. 178–188, 2016.

[4] D. Arumugam, G. Paruthimal Kalaignan, and P. Manisankar, "Synthesis and electrochemical characterizations of nano-crystalline LiFePO 4 and Mg-doped LiFePO 4 cathode materials for rechargeable lithium-ion batteries," *J. Solid State Electrochem.*, vol. 13, no. 2, pp. 301–307, 2009.

[5] C. A. Rossouw, K. Raju, H. Zheng, and K. I. Ozoemena, "Capacity and charge-transport enhancement of LFP/RGO by doping with α-MnO2 in a microwave-assisted synthesis," *Appl. Phys. A Mater. Sci. Process.*, vol. 123, no. 12, pp. 1–8, 2017.

[6] P. Benedek, N. Wenzler, M. Yarema, and V. C. Wood, "Low temperature hydrothermal synthesis of battery grade lithium iron phosphate," *RSC Adv.*, vol. 7, no. 29, pp. 17763–17767, 2017.

[7] R. Kashi, M. Khosravi, and M. Mollazadeh, "Effect of carbon precursor on electrochemical performance of LiFePO4-C nano composite synthesized by ultrasonic spray pyrolysis as cathode active material for Li ion battery," *Mater. Chem. Phys.*, vol. 203, pp. 319–332, 2018.

[8] W. Cheng *et al.*, "Preparation and characterization of LiFePO4·xLi3V2(PO4)3 composites by two-step solid-state reaction method for lithium-ion batteries," *Mater. Lett.*, vol. 198, pp. 172–175, 2017.

[9] P. C. Smecellato, R. A. Davoglio, S. R. Biaggio, N. Bocchi, and R. C. Rocha-Filho, "Alternative route for LiFePO4 synthesis: Carbothermal reduction combined with microwave-assisted solid-state reaction," *Mater. Res. Bull.*, vol. 86, pp. 209–214, 2017.

[10] Y. Z. Dong, Y. M. Zhao, Y. H. Chen, Z. F. He, and Q. Kuang, "Optimized carbon-coated LiFePO4 cathode material for lithium-ion batteries," *Mater. Chem. Phys.*, vol. 115, no. 1, pp. 245–250, 2009.

[11] S. A. Hong, S. J. Kim, J. Kim, K. Y. Chung, B. W. Cho, and J. W. Kang, "Small capacity decay of lithium iron phosphate (LiFePO4) synthesized continuously in supercritical water: Comparison with solid-state method," *J. Supercrit. Fluids*, vol.

55, no. 3, pp. 1027–1037, 2011.

[12] Y. G. Huang, F. H. Zheng, X. H. Zhang, Q. Y. Li, and H. Q. Wang, “Effect of carbon coating on cycle performance of LiFePO4/C composite cathodes using Tween80 as carbon source,” *Electrochim. Acta*, vol. 130, pp. 740–747, 2014.

[13] X. Xia, Z. Wang, and L. Chen, “Regeneration and characterization of air-oxidized LiFePO4,” *Electrochem. commun.*, vol. 10, no. 10, pp. 1442–1444, 2008.

[14] W. Gongyan, L. Li, and H. Fang, “Dehydration of Fe P O 4 ·2H 2 O for the synthesis of LiFe P O 4 /C: Effect of dehydration temperature,” *Int. J. Electrochem. Sci.*, vol. 13, no. 3, pp. 2498–2508, 2018.

[15] Y. ming Zhu, Z. wen Ruan, S. zhi Tang, and V. Thangadurai, “Research status in preparation of FePO 4 : a review,” *Ionics (Kiel).*, vol. 20, no. 11, pp. 1501–1510, 2014.

[16] P. Tang, N. A. W. Holzwarth, and Y. A. Du, “Comparison of the electronic structures of four crystalline phases of FePO4,” *Phys. Rev. B*, vol. 76, no. 17, 2007.

[17] Y. Wang, J. Wang, J. Yang, and Y. Nuli, “High-rate LiFePO4 electrode material synthesized by a novel route from FePO4 · 4H2O,” *Adv. Funct. Mater.*, vol. 16, no. 16, pp. 2135–2140, 2006.

[18] Y. Song, P. Y. Zavalij, M. Suzuki, and M. S. Whittingham, “New iron(III) phosphate phases: Crystal structure and electrochemical and magnetic properties,” *Inorg. Chem.*, vol. 41, no. 22, pp. 5778–5786, 2002.

[19] G. Schimanke and M. Martin, “In situ XRD study of the phase transition of nanocrystalline maghemite (γ-Fe2O3) to hematite (α-Fe2O3),” *Solid State Ionics*, vol. 136, no. 137, pp. 1235–1240, 2000.

[20] M. F. Ashby, “A first report x on sintering diagram,” *Acta Met.*, vol. 22, no. 3, pp. 275–289, 1974.

`

Chapter 3 Synthesize $LiFePO_4$ in an Unrestricted Environment Assisted by Gelatin as an Oxidation Protective Component

3.1 Introduction

With continually increasing on energy consumption, LIBs play a more and more important role in people's life. It has been widely used in portable electronic devices, electric vehicles, energy storage system, and so on [1]. Among different cathode materials applied in LiBs, LFP has been proved as a promising material [2]. In order to further decrease the manufacture cost of LFP, a lithiation in an unrestricted environment approach is developed and optimized in pervious chapter. The key to synthesis LFP with excellent crystallinity in short period of time is using quartz $FePO_4$ as iron source and lithium acetate as lithium source.

However, when synthesis LFP in an unstricted environment, oxidation becomes the most critical challenge for this approach [3]. Oxidation lead to a yielding of byproduct such as Fe_2O_3 and Li_3PO_4. Such impurities influence the electrochemical performance form two aspect; (1) decrease the amount of active cathode material, which is LFP, in the cell and so lead to a capacity loss. (2) decrease the electric and ionic conductivity of the cathode and so create an increasing on internal resistance that destructs the mechanism for stable input and output voltage because the extraction and insertion process for lithium ions are no longer uniform and consistent. This chapter will start with study on the oxidation process of LFP. Then a possible solution that using reduced carbon to inhibit the oxidation of LFP is proposed. A TGA analysis for six different carbon sources was conducted to find the suitable chemical for LFP synthesis. In this analysis, graphite, super P, starch, sucrose,

`

gelatin, and glucose were heated to 540 ℃ (the temperature applied for LFP synthesis) and maintained for 1 hour. Figure 3.1 is the mass versus time diagram for this heat treatment measured by a TGA. Graphite and Super P have the weight change less than 1.1%, because 540 ℃ is lower than the carbonization temperature required for them [4]–[6]. The small mass change also represents they are relatively stable at this temperature. Thus they are not suitable to be performed as sacrificial materials. On the other hand, starch is found to have a large volume expansion during decomposition. It grows to a structure composed of carbon frameworks which has larger porosity. This structure potentially brings extra pressure to designed container. And the large porosity reduces the contact surface area between carbon and oxidized LFP. This can lead to a low efficiency on regeneration of oxidized LFP. Sucrose, glucose and gelatin have similar carbon content and they are selected to be added into precursors and used for LFP synthesis.

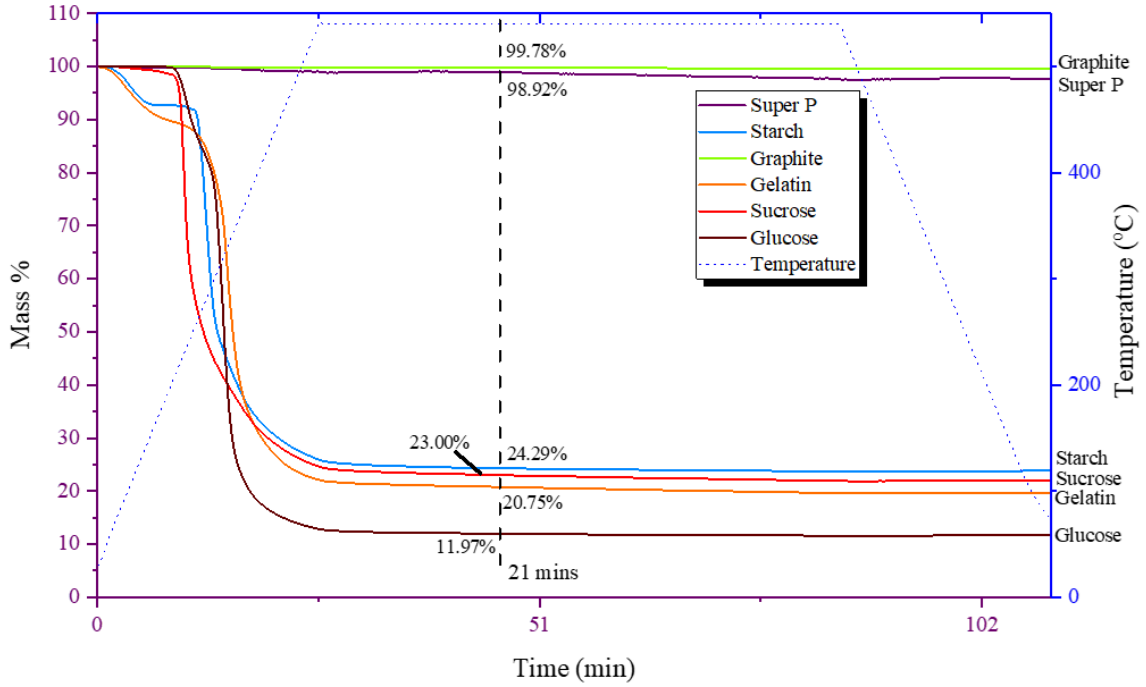

Figure 3.1. TGA results for heating , Graphite, Super P, Starch, Sucrose, Gelatin, and Glucose at 540 ℃ for 1 hour

`

3.2. Experiment procedure

Firstly, the oxidation behavior of LFP is studied by DSC and TGA via heating pristine LFP from room temperature to 600 ℃ with a heating rate of 20 ℃/min in air flow. Then, two pristine LFP samples are oxidized at 420 ℃ for 1 hour (OX-LFP420) and 600 ℃ for 4 hours (OX-LFP600), respectively. XRD is applied to characterize the oxidized phase in OX-LFP420 and OX-LFP600 to understand the oxidation process of LFP.

The precursors for LFP synthesis are based on quartz $FePO_4$ and lithium acetate. Quartz $FePO_4$ was acquired via dehydration of $FePO_4 \cdot 2H_2O$ (Sigma-Aldrich). $FePO_4 \cdot 2H_2O$ was dried in a muffle furnace at 600 ℃ for 4 hours in atmospheric environment. Anhydrous quartz $FePO_4$ powders were taken out from furnace after it was cooled to room temperature. The anhydrous α-quartz $FePO_4$ was mixed with lithium acetate in stoichiometric. 20 wt% of selected carbon source is then added into the precursors. A vertex machine was applied to uniformly mix the powders. The mixed precursors were placed in a lime glass round reaction container with special design that consider about controlling of air flow during reaction. The container was placed inside a mullite tube. The muffler furnace was preheated to 540 ℃ and the mullite tube was inserted into a muffle furnace once it reached set temperature. The tube was pulled out once the reaction finished and cooled outside at room temperature. LFP synthesized with 9, 12 ,15, 18, 21, 24 and 30mins were studied to optimize the reaction time and understand the LFP synthesis in this approach. A referenced precursor without carbon source added was also prepared and used to synthesis LFP. LFP synthesized with and without carbon source are assembled into battery cells, respectively. The schematic diagram for cell assembly is

`

demonstrated in Figure 3.2. The size of the cell case is CR2032, inside which are spring, spacer, lithium anode, celgard separator, and cathode prepared in lab. The cathode is prepared base on 85 wt% of synthesized LFP and 15% of binder polyvinylidene fluoride (PVDF). The mixture is dissolved into N-Methyl-2-pyrrolidone (NMP) with a ratio of 3.2 ml per gram of mixture. The formed solution is stirred in 600 rpm for 2 hours and doctor bladed on an Al sheet and dried at 120 ℃ for 48 hours to make the cathode ready to be tested. An Arbin tester is applied to test the electric performance of assembled battery cells. Except Arbin tester, XRD is applied to obtain the crystalline phase of resulted LFP. The particle size and morphology are observed via a SEM.

`

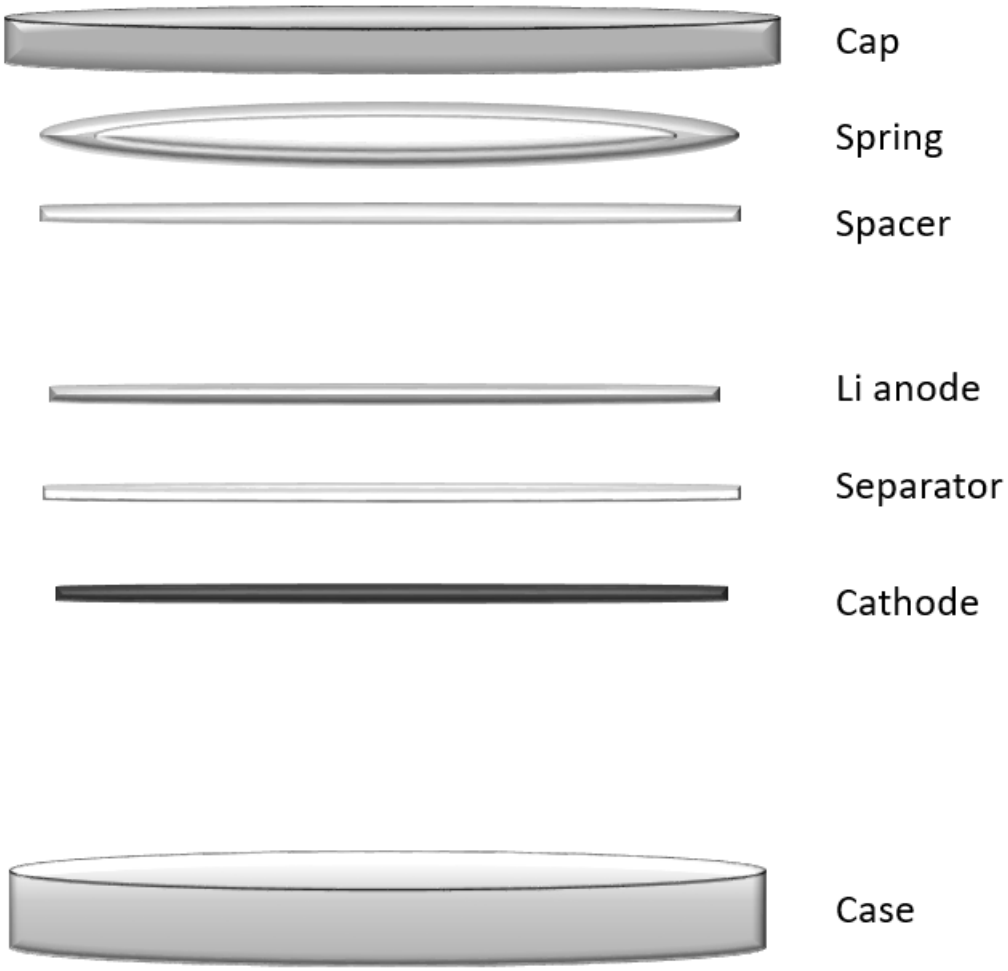

Figure 3.2. The schematic diagram for battery cell assembly

`

3.3 Result and discussion

The research of this chapter can be separated to two aspects. Firstly, the oxidation behavior of LFP is studied to understand the oxidation process and investigate the possible roles that carbon can play for protecting LFP from oxidation. Then LFP is synthesized with carbon added and characterized to investigate the effectiveness of using carbon to inhibit the oxidation and understand the progress it takes carbon source to limit oxidation.

3.3.1 Oxidation of LFP

Figure 3.3 is the TGA and DSC results for heating pristine LFP/C (MTI corporation) from room temperature to 600 ℃ with the heating rate of 20 ℃/min. It demonstrates the process of LFP/C oxidation. The first slope in TGA before 30 ℃ is evaporation of moisture corresponding with 0.3% loss on weight. LFP/C oxidation process starts at 300 ℃. O atom acquire enough internal energy at this temperature, start to overcome the active energy and diffuse into the LFP/C. LFP start to loses the crystallinity and reach the first DSC peak at 420 ℃ with 1% of weight increase. Then, the bond between carbon coating and LFP start to broke [7]. Because carbon is coated on the surface of LFP particles, it firstly reacts with oxygen and results with CO_2 releasing. The 1.4% weight loss between 420 ℃ and 550 ℃ represents this pristine LFP/C has a carbonization rate about 1.4%. This value matches with its Materials Safety Data Sheet (MSDS) [8]. With carbon coating evaporated, oxygen start to diffuse into LFP. The oxidation of LFP is corresponded to the second exothermic peak at 560 ℃ in DSC. As more and more oxygen reacted with LFP, about 1.4% weight increment is observed form 560 ℃ to 600 ℃.

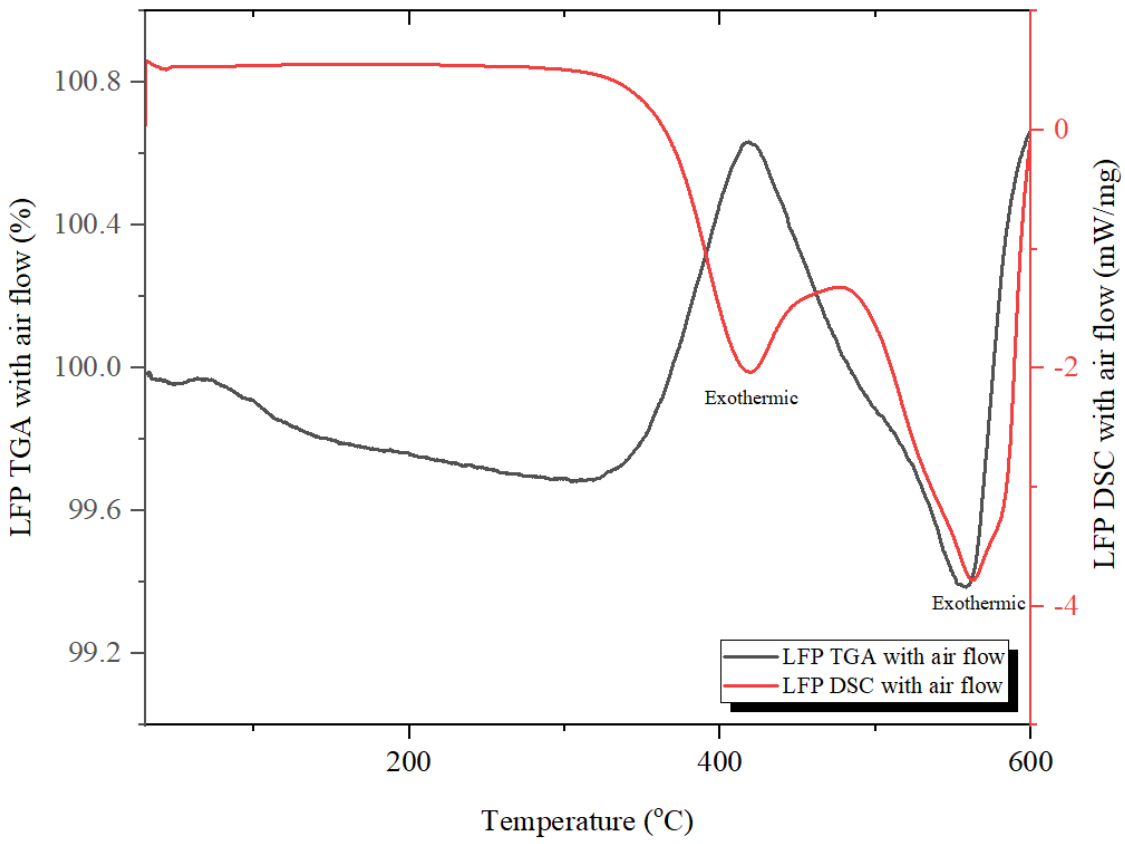

Figure 3.3 The TGA and DSC results of heating LFP from room temperature to 600 ℃ in air flow

`

The XRD results demonstrated in Figure 3.4 is a corroboration for above introduction. Pristine LFP/C is heated in atmospheric environment at 420 ℃ for 1 hour (OX-LFP420) and 600 ℃ for 4 hours (OX-LFP600), respectively. OX-LFP420 is able to maintain the LFP patterns because oxygen is firstly reacted with carbon coating as mentioned previously. This result confirmed that carbon can be used as a sacrificial material and protect LFP from oxidation. However, LFP also start to lose crystallinity at this temperature. It is reflected by the intensity ratio change between the main peaks of LFP. Iron oxide peaks start to show up. This demonstrates that with temperature increasing, crystal start to change partially. O_2 that diffused into LFP crystal partially oxidized LFP and start to form iron oxide. On the other hand, with higher heating temperature and longer heating time, LFP is further oxidized and resulted with formation of $Li_3Fe_2(PO_4)_3$ which is demonstrated in the XRD pattern of OX-LFP600. Noticed that although $Li_3Fe_2(PO_4)_3$ can also be used as cathode material for LiBs, it has lower working voltage and less capacity than LFP [9]. Therefore, it still decreases the performance of LFP based cathodes.

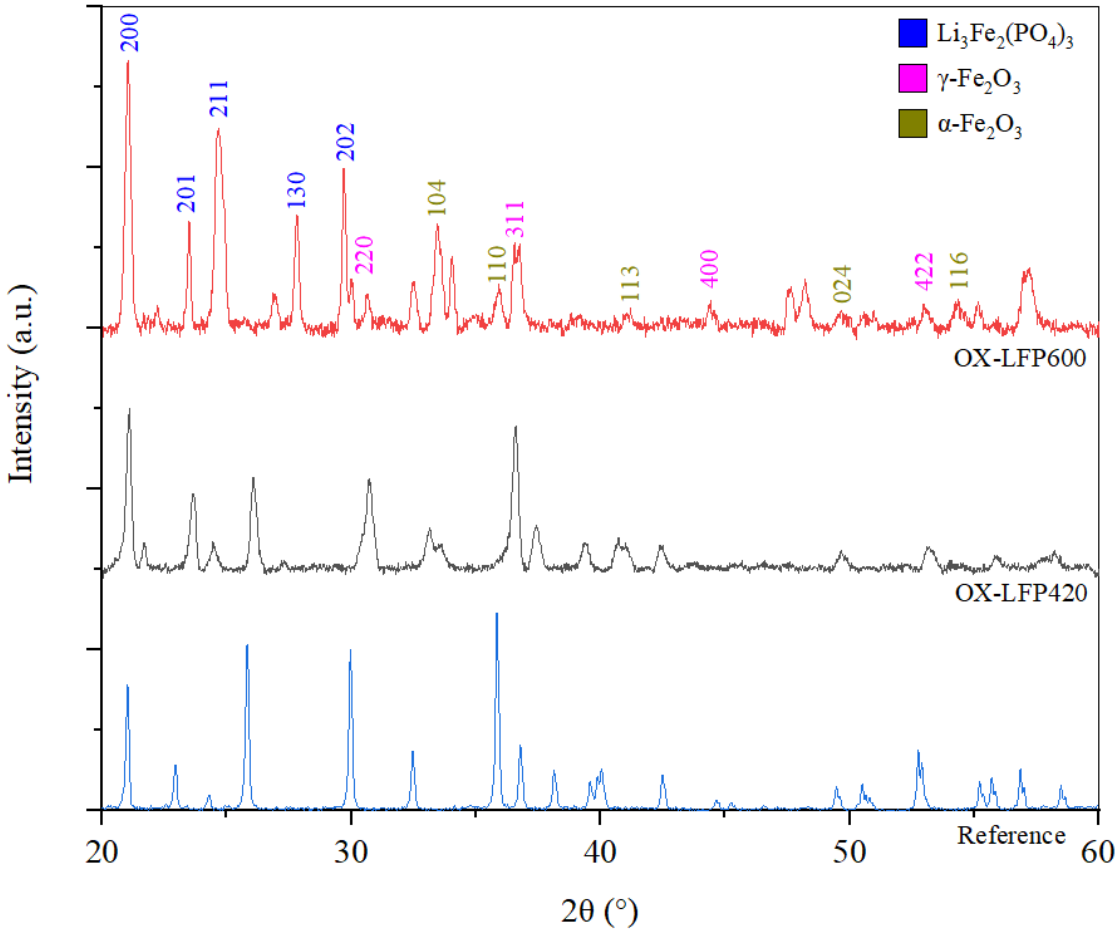

Figure 3.4. XRD pattern for LFP420 and LFP600

`

Base on the XRD result, the oxidation reaction can be concluded as follow:

$$12LiFePO_4\ (s) + 3O_2\ (g) \rightarrow 4Li_3Fe_2(PO_4)_3\ (s) + 2Fe_2O_3(s)$$

The weight increment is come from O_2 reacted with LFP, and the percentage it increases is:

$$Wt\% = \frac{3 \times N_{O_2}}{12 \times N_{LFP}} = 5\%$$

According to the TGA result in Figure 3.3, the weight increment in real is 1.4%, meaning about 28% of LFP is oxidized.

Figure 3.5 demonstrates the SEM result for pristine LFP/C. Most LFP particles have a micrometer size. Large particles can be 6 to 8 μm. The large particles size keeps the LFP from fully oxidation. On one hand, at 600 ℃, O atom does not have enough internal energy to diffuse into the center of micro-size LFP, on the other hand, the formed $Li_3Fe_2(PO_4)_3$ becomes a passivation layer and protects the rest of LFP from further oxidation. This is the reason both XRD and TGA demonstrate that only part of LFP is oxidized in OX-LFP600. As introduced in Chapter 1, the lithiation in an unrestricted environment approach is developed base on solid state approach [10], [11]. This kind of approach is featured with synthesizing LFP in micro size. This make it perfected to be optimized, modified, and then conduct the LFP synthesis process (lithiation) in an unrestricted environment.

`

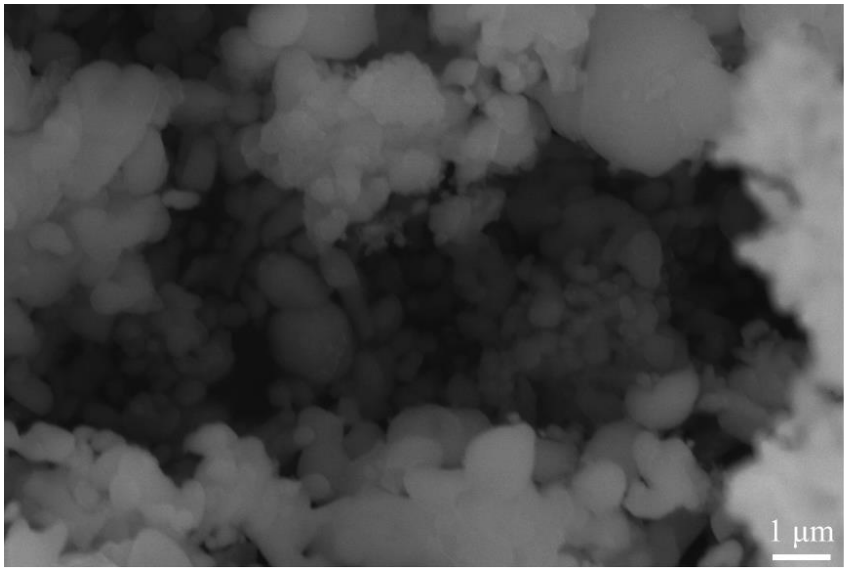

Figure 3.5. The SEM result for pristine LFP

Oxidation can also occur during the growth of LFP crystal. The smaller particle size of LFP at this stage leads to a fully oxidation and yielding of by product. As discussed previously, the byproduct can be Li_3PO_4 and Fe_2O_3. The oxidation occurred here is more difficult to limit since is conducted nearly simultaneously with LFP synthesis. However, the oxidized LFP is able to be recovered. Xin Xia *etal.* utilized polypyrrole (PPy) to regenerate the oxidized LFP [12]. The regeneration transforms the α-Fe_2O_3, $FePO_4$ and Li_3PO_4 back to $LiFePO_4$ at 400 °C:

$$3C\ (s) + 4Li_3PO_4\ (s) + 2Fe_2O_3\ (s) + 8FePO_4(s) \rightarrow 12LiFePO_4\ (s) + 3CO_2\ (g)$$

Therefore, a carbon added lithiation in an unrestricted environment process is proposed in this research to solve the oxidation issue. Beside the $FePO_4$ and lithium acetate, carbon source is also added into precursors. It will perform two roles during reaction. Firstly, it is the sacrificial material which consume the oxygen inside the reaction chamber. Since the

`

reaction chamber is closed during LFP synthesis, carbon added will decrease the partial pressure of oxygen inside the chamber and so limits oxidation. Secondly, it will be applied to regenerate oxidized LFP during synthesis in an unrestricted environment. In this research, carbon source has a high carbon content and low fabrication cost will be firstly considered to add into precursors. Then the effect of adding carbon source into precursors is then investigated. Study is also done to understand the carbon added synthesis process.

3.3.2 Synthesis LFP with adding of carbon source

LFP is then synthesized with sucrose, glucose and gelatin, respectively. The resulted powders were characterized by XRD and demonstrated in Figure 3.6. It is found that LFP synthesized with glucose, gelatin, and sucrose all result with crystalline LFP meaning 20 % of carbon source has insignificant impact on the crystallinity of synthesized LFP. On the other hand, the peaks for byproduct are also demonstrated in all the patterns, meaning side reaction (oxidation) is still triggered during LFP synthesis. Except the small different on effect of γ-Fe_2O_3 inhibition which can be observed by comparing (220) and (400) peak, in general, the different between LFP synthesized with glucose, gelatin, and sucrose is not significant in the view of XRD patterns. Although some peaks such as (104) or (400) demonstrate that they also have small discrepancy on LFP oxidation level, but such little difference on peak can due to the baseline corrections. LFP synthesized with gelatin is selected because of the cost effectiveness for gelatin. G. It is going to be compared with LFP synthesized without carbon source added to evaluate its ability to inhibit oxidation.

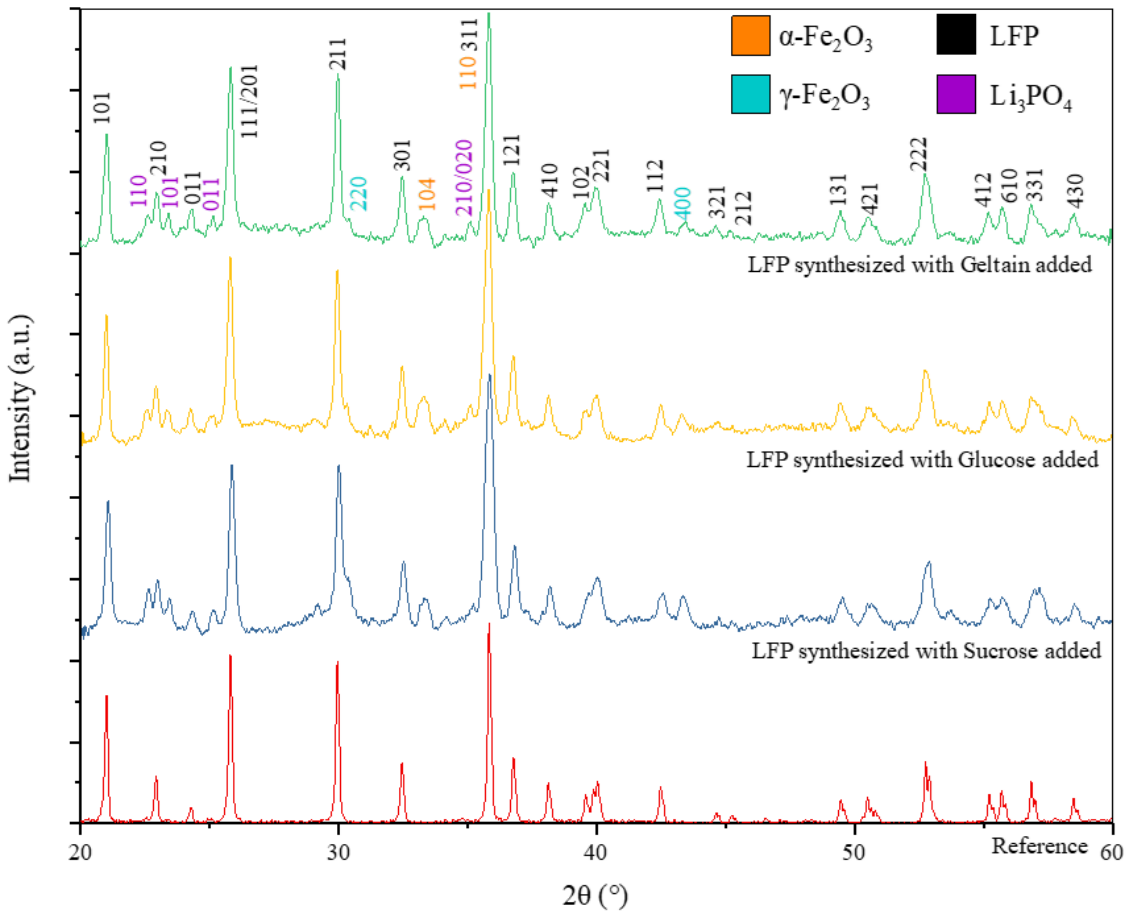

Figure 3.6. XRD pattern for LFP synthesized with gelatin, glucose and sucrose

`

Figure 3.7 is the XRD patterns for LFP synthesized with and without gelatin. A significant difference can be observed between the LFP synthesized with and without carbon source (gelatin) added. Apparently, crystalline LFP is synthesized no matter with or without carbon source added when the peak position and peak to noise ratio of (101), (111/201), (211) and (311) are considered. However, the oxidation is limited especially consider the ratio between (104) from α-Fe_2O_3 and (301) peaks from LFP. This intensity ratio is related with mole ratio by the following equation via assuming the powder is well mixed and micro-absorption of X-rays are neglected:

$$\frac{I_{LFP(301)}}{I_{\alpha\text{-}Fe_2O_3(104)}} = K\frac{X_{LFP}}{X_{\alpha\text{-}Fe_2O_3}}$$

Where X is the mole fraction of related species in the synthesized LFP mixture. K is the constant depend on the peaks select to compare, component of phases, the diffraction line, and the mass absorption coefficient of the species present. With K remain unknown, the mole fraction of each component is not able to be calculated in LFP either synthesized with or without carbon source added. However, in consider the mole fraction ratio of LFP and α-Fe_2O_3:

$$R = \frac{X_{LFP}}{X_{\alpha\text{-}Fe_2O_3}}$$

There are:

$$R_{\text{with carbon}} = \frac{X_{\text{LFP with carbon}}}{X_{\alpha\text{-}Fe_2O_3\ \text{with carbon}}}$$

`

$$R_{\text{without carbon}} = \frac{X_{\text{LFP without carbon}}}{X_{\alpha\text{-}Fe_2O_3 \text{ without carbon}}}$$

And so:

$$\frac{R_{\text{with carbon}}}{R_{\text{without carbon}}} = \frac{I_{\text{LFP(301) with carbon}}}{I_{\alpha\text{-}Fe_2O_3\,(104) \text{ with carbon}}} \times \frac{I_{\alpha\text{-}Fe_2O_3\,(104) \text{ without carbon}}}{I_{\text{LFP(301) without carbon}}}$$

The unknown constant K is reduced and since the intensity for the (301) from LFP is almost remain same, it can be conducted:

$$\frac{R_{\text{with carbon}}}{R_{\text{without carbon}}} = \frac{I_{\alpha\text{-}Fe_2O_3\,(104) \text{ without carbon}}}{I_{\alpha\text{-}Fe_2O_3\,(104) \text{ with carbon}}} \approx 2$$

With adding of carbon source, the mole fraction ratio of LFP and α-Fe_2O_3 is doubled. Although the specific value for mole fraction of LFP and α-Fe_2O_3 remain unknown, a significant decrease on α-Fe_2O_3 can be observed. And in summary, XRD patterns represent carbon source added successfully performed as sacrificial material and regeneration agent. As a result, crystalline LFP with less oxidation is synthesized with adding of gelatin. And since LFP synthesized with sucrose and glucose have similar quality, this conclusion can also be applied for sucrose and glucose. It is inferred that the approach of adding carbon source to protect LFP from oxidation will be effect for variety of carbon source.

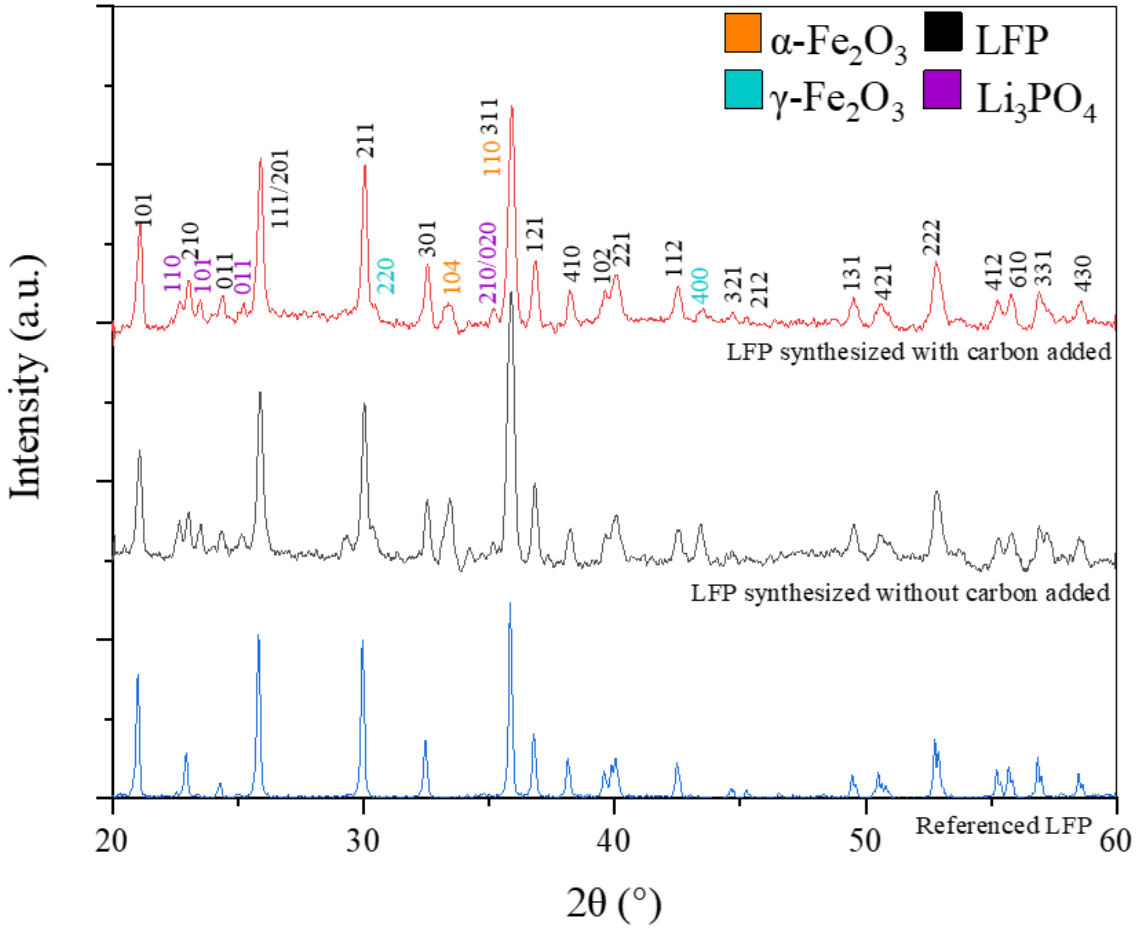

Figure 3.7. XRD pattern for LFP synthesized with and without Gelatin

`

In order to demonstrate the discrepancy on the quality of LFP synthesized with or without carbon added, two battery cells are assembled with LFP cathode that synthesized with and without Gelatin. They are denoted as Cell-Gelatin and Cell-NC, respectively. Figure 3.8 is the charge and discharge curve for these two battery cells. As the figure illustrated, Cell-NC has a poor performance because the voltage cannot be hold during discharge and so it has a very low discharge capacity about 16 mAh/g. The low capacity is due to the higher oxidation of LFP demonstrated in the Figure 3.7. While in the case of Cell-Gelatin, a flat charge at 3.5 V and discharge at 3.4 V is observed, meaning it has a stable input and output voltage. It shows a discharge capacity of 136 mAh/g which reaches to 80% of its theoretical capacity, 170 mAh/g [13]. Although Cell-NC has a start capacity of 136, it has an issue of fast fading. Figure 3.9 (a) is the discharge capacity and coulombic efficiency by cycle number for Cell-Gelatin. The discharge capacity is decreased to 90 mAh/g at 36th cycle, which is 66% of the first cycle. The coulombic efficiency is lower than 80% in this case. This fast fading rate can also be observed in Figure 3.9 (b). Both charge and discharge curve quickly move to the left with increasing on cylce number. These all indicate the fading process of LFP is in a high rate. This kind of fading is caused by the impurty phase, which is the byproduct of LFP oxidition, inside the cathode. Lithium ion in this case is traped with the interstitial sites and dislocations of low conductivity impurties, such as α-Fe_2O_3. More and more ions are trapped with the cycle of charging and discharging which then lead less and less lithium ions are activated. With less lithium ions available, capacity of Cell-Gelatin quickly fades and this is the reason the charging and discharging curve is moving to the left in Figure 3.9 (b).

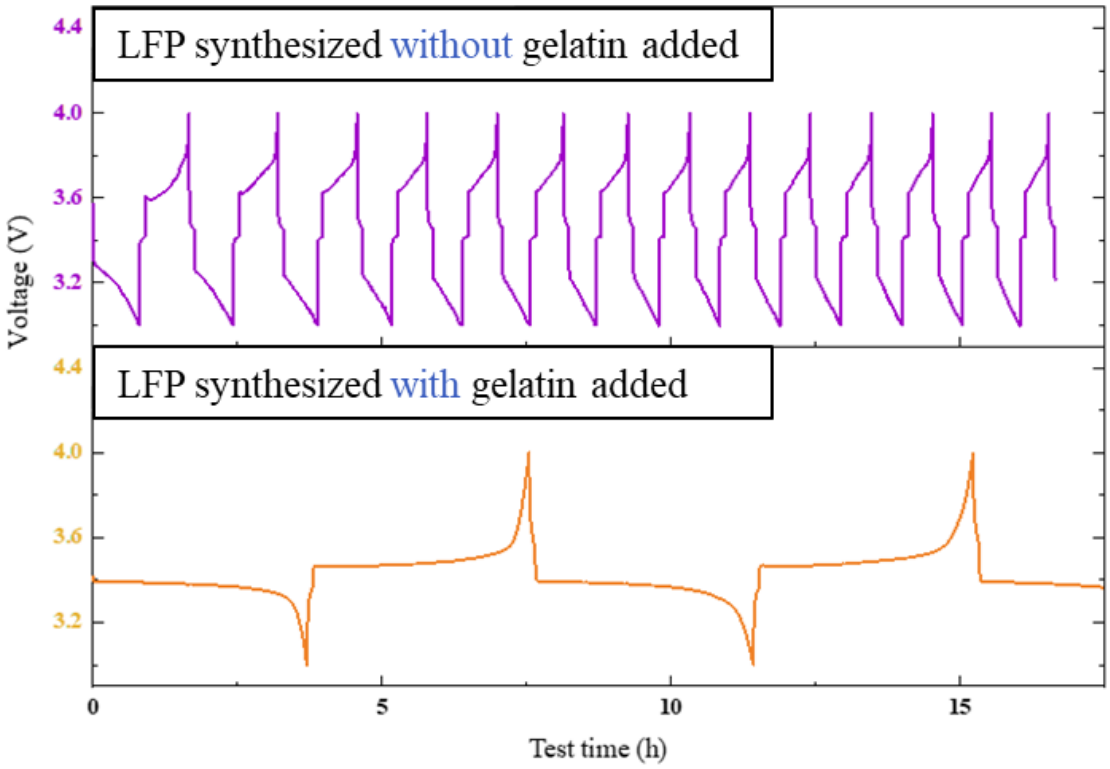

Figure 3.8. The charge and discharge curve for battery cells assembled with LFP cathode synthesized with Gelatin (Cell-Gelatin) and without gelatin (Cell-NC)

(a)

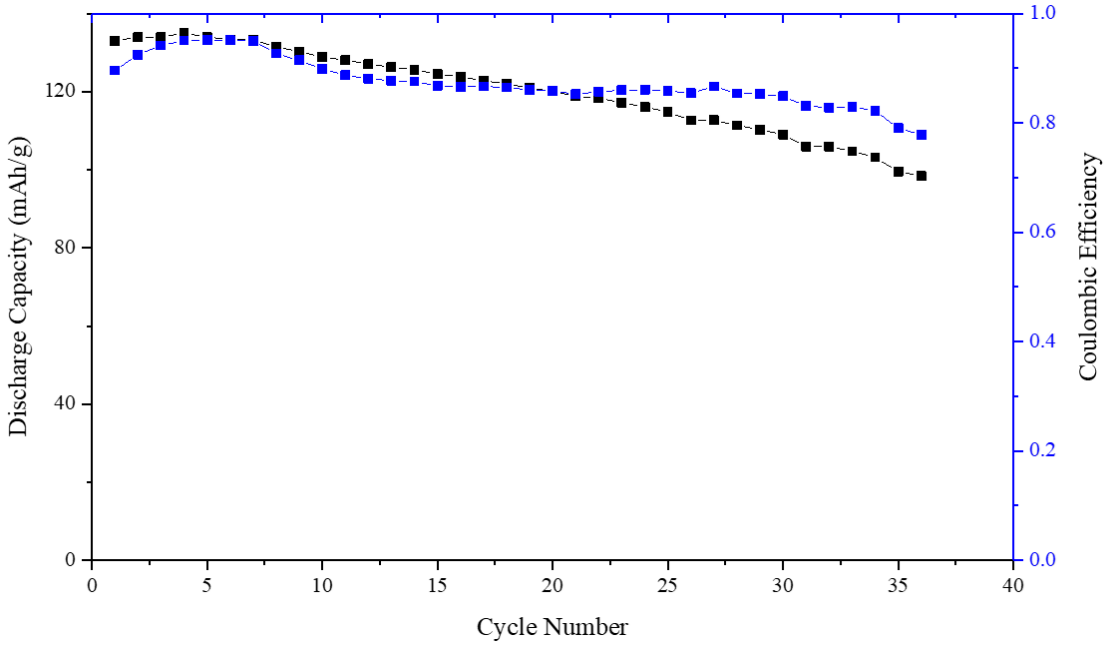

(b)

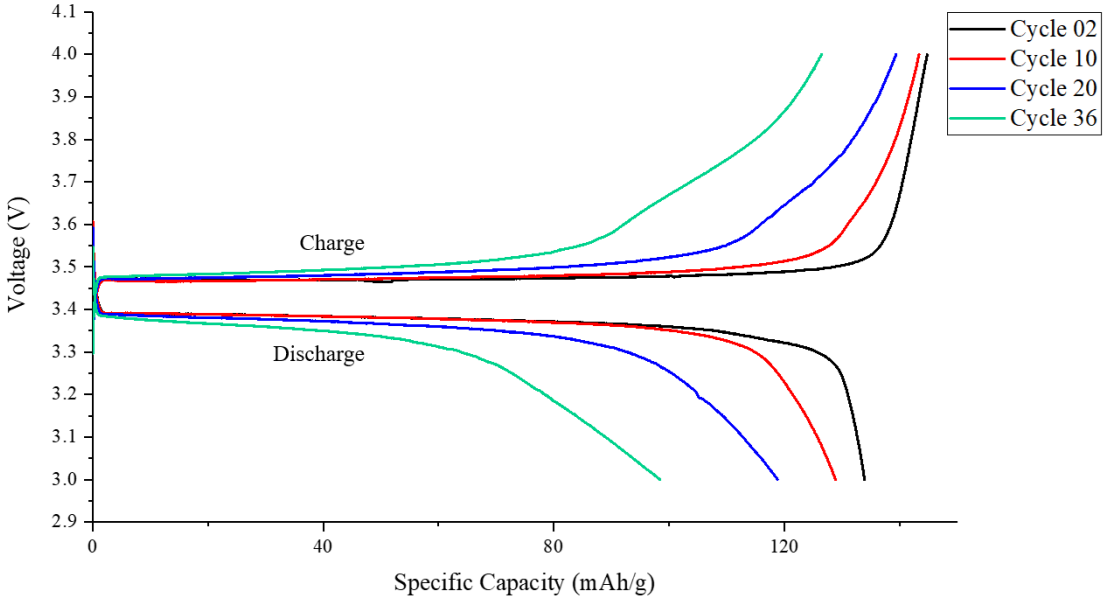

Figure 3.9. The (a) discharge capacity and coulombic efficiency and (b) charge and discharge capacity verse cell voltage, by cycle number for Cell-Gelatin

`

Figure 3.10 is the XRD pattern for LFP/C synthesized in 0 (which is the mixture of precursors) 9, 12, 15, 18, 21, 24 and 30 minutes. They are denoted as LFP00, LFP09, LFP12, LFP15, LFP18, LFP21, LFP24 and LFP30, respectively. All of them are synthesized with 20wt% of gelatin added. LFP synthesized in 9 mins has already showed a clear LFP peaks, meaning lithiation approach applied in this research has a high reaction rate when compare to traditional solid state reaction approach. Previous chapter has demonstrated that the feature of lithium acetate accelerates the lithiation process to produce LFP. The XRD patterns showed here demonstrate that the reaction rate for LFP synthesis is higher than previous estimation. The forming of crystalline LFP crystal in this case is finished in 9 mins. The peak that shows more obvious change on intensity is iron oxide peak which is (104). It can also start to be observed from LFP09. Due to the unrestricted environment, LFP is oxidized while synthesizing. And is very likely to occur at the beginning state of LFP crystal growth and it has a high rate under reaction temperature, 540 ℃. However, the intensity of (104) is decreasing while synthesis time increasing. This shows that gelatin starts to work as a reducing agent, and similar to pervious discussion, the mole fraction ratio between (301) from LFP and (104) from α-Fe_2O_3 is decreasing, meaning the oxidation is inhibited. This process is slower than LFP synthesis and so needs an extra reaction time such as 30 mins.

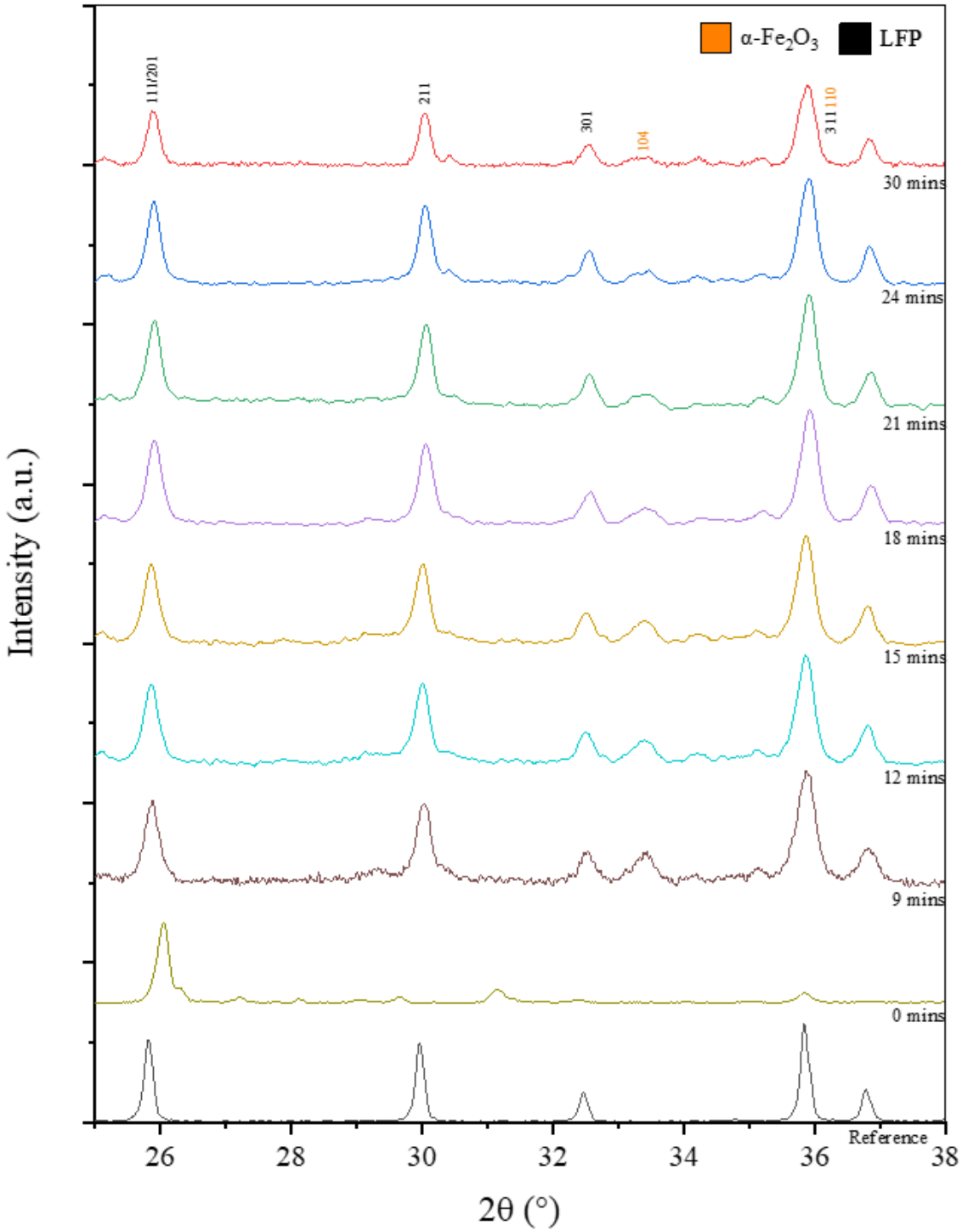

Figure 3.10. XRD pattern for LFP synthesized in different time

`

Figure 3.11 is the TGA and DSC results for gelatin decomposition from 0 to 600 ℃. As it illustrated, decomposition of gelatin can be divided into three stages. The first stage, corresponded with the first DSC peak around 100 ℃, is dehydration. During this step, 10 to 15% of weight is lost. Water bound to gelatin can be divided into three different types (1) water bound by high-energy sorption centers that occurs inside collagen triple helix and which plays a major role in its stabilization by intramolecular bonds, the amount of water depending on the degree of helicity of the macromolecules. (2) water absorbed by polar groups of gelatin and collagen macromolecules, bound to proteins by hydrogen bonds, located outside the helical fragments and also contributing to the stabilization of the collagen helical structure. The amount of this water in gelatin probably corresponds to the mono-molecular layer and can be considered as structural water. (3) water absorbed by proteins to give poly-molecular layers, consisting of the total amount of water bound in gelatin and the amount of structural water [14]. Because water in gelatin can exist in these three forms, it usually has 10 to 15% on weight. Protein denaturation also occurs in this stage. The denaturation causes protein to loss its quaternary structure, tertiary structure, and secondary structure. However, no chemical bond broken is triggered at this stage and so no weight loss is related to denaturation.

Then, above 200 ℃, the protein degradation starts [15]. Firstly, peptide bonds broke, corresponding with the DSC peak at 230 ℃ and very small change on TGA. Protein degraded to polypeptides and then thermally decomposed to amino acid. Then, start from 230 ℃, a significant weight losing can be observed. In this step, DSC curves contains peak which is corresponded to the thermal degradation process for different amino acid. The

`

peak is composed by several small peaks due to the different degradation temperature that different amino acids have. Degradation of amino acid occurs associated with broking of C-O, C-N bond and releasing of gases. For example, gelatin usually contains 20 to 30% of glycine which is the most among all amino acids in gelatin. The degradation reaction can be concluded as [16]:

$$4(C_2H_5NO_2)\ (s) \rightarrow 6H_2O\ (g) + 2NH_3\ (g) + 6C\ (s) + 2(CHNO)\ (s)$$

I this case, the significant weight drop can be concluded as the releasing of H_2O and NH_3 during degradation. The peptide bonds cleavage and amino acid degradation together, compose the stage of protein degradation.

Finally, start form 500 ℃, a huge drop is observed on DSC curve. This is a sign for the third decomposition stage, thermal decomposition, for gelatin. This represents the decomposition of organic matters formed during degradation of amino acid, such as CHNO or $C_2H_2N_2O_2$ produced by the decomposition of glycine. Also, it should be noticed that the synthesis temperature applied in this reaction, 540 ℃, is in this zone.

Here, the carbon formed in protein degradation stage can be applied to protect LFP from oxidation by the regeneration process mentioned previously:

$$3C\ (s) + 4Li_3PO_4\ (s) + 2Fe_2O_3\ (s) + 8FePO_4(s) \rightarrow 12LiFePO_4\ (s) + 3CO_2\ (g)$$

It should be noticed, as demonstrated in chapter 2, lithium acetate decomposed around 400 ℃:

$$2CH_3COOLi\ (l) \rightarrow Li_2O\ (s) + 3H_2O\ (g) + 4C\ (s)$$

This decomposition process also release carbon. However, according to Figure 3.3, when LFP firstly starts to oxidize on 350 ℃, the lithium acetate is still in liquid state. Carbon

`

yielded via amino acid degradation, can produce a reduced atmosphere under relatively low temperature range and so limited the produce of byproduct via oxidation. However, it still consumes some time for gelatin decomposition. And as mentioned previously, LFP synthesized with gelatin needs certain amount of time for regeneration of oxidized LFP. and starts to work as a reduce agent. This is the reason LFP30 is preferred since it has a longer reaction time.

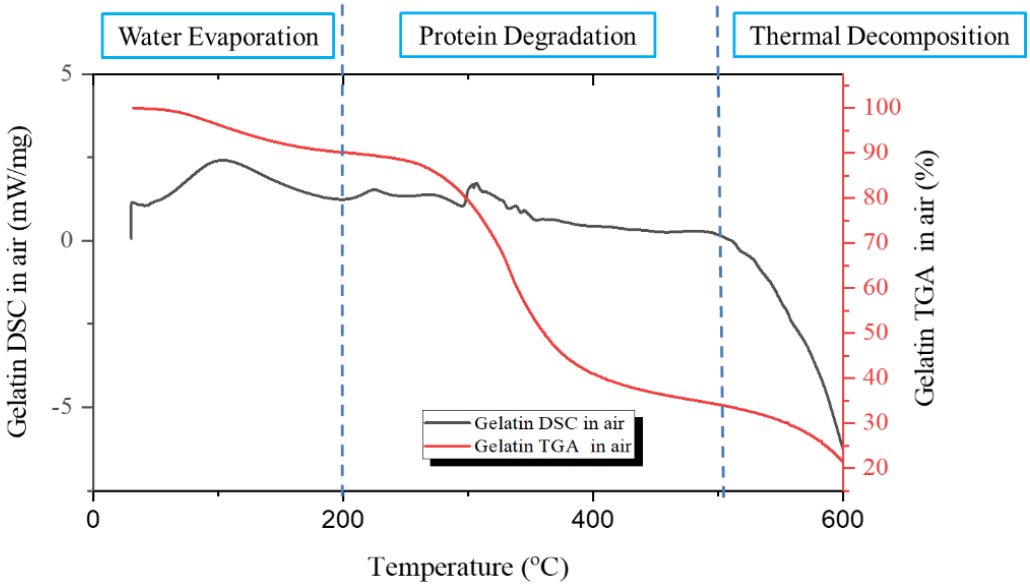

Figure 3.11. The TGA and DSC results for gelatin decomposition from 0 to 600 ℃

`

Figure 3.12 the SEM results for LFP09, LFP15, and LFP24. These three samples are selected and characterized to investigate the morphology change while synthesis time increasing. Firstly, as they demonstrated, when considered on the level of 300 nm, the grain size is not uniform. The size is varied from 100 nm to 1,000 nm. This is mainly due to unperfected mixing of precursors. Secondly, from LFP09 to LFP24, clearer particle, smaller average particle size, and smaller size variance can be observed. The size is distributed from 50 nm to even several micros. These all pointed that growth of LFP grain takes time, at least longer than 9 mins, although LFP has already formed at this time.

`

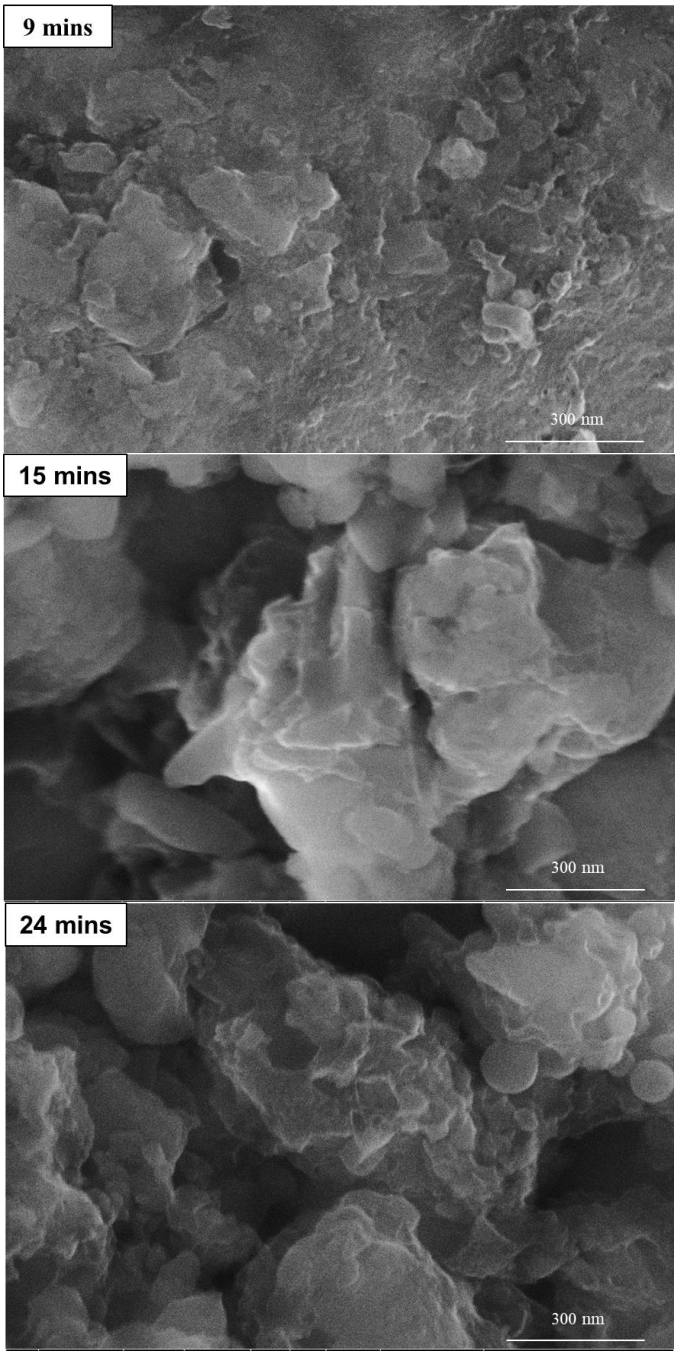

Figure 3.12. The SEM results for LFP09, LFP15, and LFP24

`

3.4 Conclusion

Oxidation of LFP is the main issue faced during development of lithiation in an unstricted environment for LFP synthesis. This oxidation can be triggered at relatively low temperature range. Gelatin added as a carbon source degraded even below this temperature range. The carbon released in the degradation process produce a reduced atmosphere and so protect the LFP from further oxidation. As a result, using gelatin inhibits the yielding of impurity phase via oxidation during LFP synthesis. It also significantly improves the electrochemical performance of the battery cell whose cathode is based on synthesized LFP. As a summary, longer synthesis time is required because of two reasons. 1) gelatin need time to reduce the overreacted LFP to work as a reduce agent and so inhibit LFP oxidation. 2) LFP grain need time to growth and reach a more uniform distribution on size. LFP synthesized in 30 mins in this case has the best quality on the aspects of purity and grain growth.

`

Reference:

[1] P. K. Nayak *et al.*, “Review on Challenges and Recent Advances in the Electrochemical Performance of High Capacity Li- and Mn-Rich Cathode Materials for Li-Ion Batteries,” *Adv. Energy Mater*, vol. 1702397, no. 8, pp. 1–16, 2018.

[2] R. P. Rao, M. V Reddy, S. Adams, and B. V. R. Chowdari, “Preparation , temperature dependent structural , molecular dynamics simulations studies and electrochemical properties of LiFePO 4,” *Mater. Res. Bull.*, vol. 66, pp. 71–75, 2015.

[3] D. Larcher, C. Masquelier, D. Bonnin, Y. Chabre, and V. Masson, “Effect of Particle Size on Lithium Intercalation into α-Fe2O3,” *J. Electrochem. Soc.*, vol. 150, no. 1, pp. 133–139, 2003.

[4] M. Klett, T. G. Zavalis, M. H. Kjell, R. W. Lindström, M. Behm, and G. Lindbergh, “Electrochimica Acta Altered electrode degradation with temperature in LiFePO 4 / mesocarbon microbead graphite cells diagnosed with impedance spectroscopy,” *Electrochim. Acta*, vol. 141, pp. 173–181, 2014.

[5] Q. Fan, L. Lei, Y. Chen, and Y. Sun, “Biotemplated synthesis of LiFePO 4 / C matrixes for the conductive agent-free cathode of lithium ion batteries,” *J. Power Sources*, vol. 244, pp. 702–706, 2013.

[6] X. Zhi, G. Liang, L. Wang, X. Ou, L. Gao, and X. Jie, “Optimization of carbon coatings on LiFePO 4 : Carbonization temperature and carbon content,” *J. Alloys Compd.*, vol. 503, no. 2, pp. 370–374, 2010.

[7] R. Dominko, M. Bele, M. Gaberscek, M. Remskar, D. Hanzel, and S. Pejovnik, “Impact of the Carbon Coating Thickness on the Electrochemical Performance of LiFePO4/C Composites,” *J. Electrochem. Soc.*, vol. 152, no. 3, pp. 607–610, 2005.

[8] MTI Corporation, “Safety Data Sheet Lithium iron(II) phosphate.” pp. 1–6, 2018.

[9] H. Karami and F. Taala, “Synthesis , characterization and application of Li3 Fe2 (PO4)3 nanoparticles as cathode of lithium-ion rechargeable batteries,” *J. Power Sources*, vol. 196, no. 15, pp. 6400–6411, 2011.

[10] C. H. Mi, G. S. Cao, and X. B. Zhao, “Low-cost , one-step process for synthesis of carbon-coated LiFePO4 cathode,” *Electrochim. Acta*, vol. 59, pp. 127–130, 2005.

[11] P. C. Smecellato, R. A. Davoglio, S. R. Biaggio, N. Bocchi, and R. C. Rocha-Filho, “Alternative route for LiFePO4 synthesis: Carbothermal reduction combined with microwave-assisted solid-state reaction,” *Mater. Res. Bull.*, vol. 86, pp. 209–214, 2017.

[12] X. Xia, Z. Wang, and L. Chen, “Regeneration and characterization of air-oxidized LiFePO4,” *Electrochem. commun.*, vol. 10, no. 10, pp. 1442–1444, 2008.

`

[13] W. Zhang, “Structure and performance of LiFePO4 cathode materials : A review,” *J. Power Sources*, vol. 196, no. 6, pp. 2962–2970, 2011.

[14] I. Yakimets, N. Wellner, A. C. Smith, R. H. Wilson, I. Farhat, and J. Mitchell, “Mechanical properties with respect to water content of gelatin films in glassy state,” *Polymer (Guildf).*, vol. 46, pp. 12577–12585, 2005.

[15] P. L. M. Barreto, A. T. N. Pires, and V. Soldi, “Thermal degradation of edible films based on milk proteins and gelatin in inert atmosphere,” *Polym. Degrad. Stab.*, vol. 79, pp. 147–152, 2003.

[16] I. M. Weiss, C. Muth, R. Drumm, and H. O. K. Kirchner, “Thermal decomposition of the amino acids glycine , cysteine , aspartic acid , asparagine , glutamic acid , glutamine , arginine and histidine,” *Weiss al. BMC Biophys.*, vol. 11, no. 2, pp. 1–15, 2018.

`

Chapter 4 Development of an Auto Pressure Release Method for One Step Synthesis of LFP/C in an Unrestricted Environment

4.1 Introduction

In previous chapter, LFP has been successfully synthesized via a lithiation in an unrestricted environment. By adding gelatin as a carbon source, the oxidation of LFP is controlled and minimized. However, there are three issues remaining.

Firstly, LFP, since it has a low ionic and electronic conductivity, need to be smaller in particle size, carbonized, or doped with conductive metal element [1]. And because gelatin has already been added into precursors in previous study, applying carbonization and combine it with LFP synthesis in single step will be the most efficient approach to improve its conductivity. Therefore, the synthesis temperature and heating time will be both increased to make sure LFP can be well carbonized [2]. An excess number for synthesis temperature and heating time is set without further optimization in order to acquire LFP with highest quality.

Secondly, previous system designed for LFP synthesis is a closed system. There is no substance exchange between synthesis system and outer environment. Although increasing the scale of precursors does not reduce the quality of synthesized LFP, it does significantly increase the inner pressure for the current closed system because more gas, such as water vapor and CO_2, is released during synthesis reaction. This brings a strong challenge to either improve the pressure resistance for current reaction chamber or significantly increase the size of reaction chamber with scaling up. Both strength and size of the reaction chamber in this case limited the scale for LFP synthesis. Therefore, a modified reaction setting, an

`

auto pressure release method (APR) is proposed in this chapter. The design idea is basically allowing the gas inside reaction chamber to flow to the outside environment because of the pressure gradient while prevent the gas exchange between inner and outer.

With the two issues solved, optimization will be done to further improve the quality of LFP. Currently, modification and enhancement have been applied to the LFP synthesis setup to reduce the oxidized LFP or offer a reduced atmosphere to prevent the LFP form reacting with oxygen. However, this approach is not able to fully remove the oxidation. So, the effort need to be done from another aspect, that is to limit the amount of oxidant via controlling vapor pressure. A setup modification is used to decrease the partial pressure of oxidant without external device (such as heavy duty pump) assistance. Here, water is used as sacrificial material while the muffler furnace is heating. The water evaporated increases the inner gas pressure and creates pressure gradient from inner of chamber to outer environment. Gases contains oxygen originally existed in the chamber flow to the outside environment. It will result with a much lower equilibrium partial pressure for oxygen and so decrease the amount of oxidant available for LFP oxidation.

About the possibility of oxidizing LFP by water vapor, K. Zaghib *et al.* suggested that delithiation is observed in the case of exposure LFP to H_2O in air, and yet, it affects only the disordered surface layer of the LFP particles [3]. Expose LFP to water result in Li_3PO_4 with a few nm thickness [4]. The more obvious aging for LFP which is caused by water vapor can be found in long term experiment. Figure 4.1 is the capacity fading of LFP in humid and dry atmosphere [5]. The 10% fading of capacity takes 6 months at room temperature (25 ℃). Fading rate increases as environment temperature increases.

`

However, even at 60 ℃, it still takes 2 months to reach 10% fading of capacity. Considered a longest 5 h process for LFP synthesis, the influence of water vapor on LFP quality should be nonsignificant.

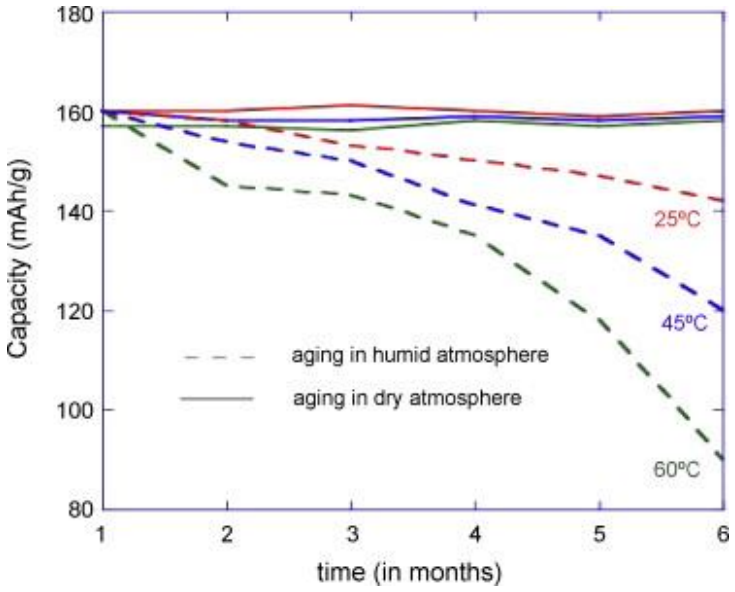

Figure 4.1. The capacity fading of LFP in humid and dry atmosphere

`

4.2 Experiment procedure

In order to carbonize LFP and enhance its ionic and electric conductivity, a reaction temperature (750 ℃) and longer reaction time (5 hours) are applied here. A quartz boat is applied instead of lime glass tubular reaction vessel which is used in pervious experiment since lime glass melted around 560 ℃. Besides that, LFP is still synthesized via a mixture of $FePO_4$, lithium acetate and gelatin. $FePO_4$ and lithium acetate are mixed in stoichiometry, and 20% of gelatin in weight is added into it. The mullite tube was inserted into a muffle furnace once it reached to the reaction temperature, 750 ℃, and maintained for 5 hours. The tube was pulled out once the reaction finished and then cooled down to the room temperature.

In order to scale-up synthesis, experiment setup is modified as demonstrated in Figure 4.2, an APR is added into pervious LFP synthesis setup. Instead of a sealed reaction chamber, valve is left open to allow the gas to be purged out to the outside environment. The driving force for flowing is the pressure gradient created by releasing of H_2O and CO_2 during synthesis reaction and the high temperature applied in the reaction chamber. The gas will flow through a rubber catheter and arrive to a beaker filled with DI water which is degassed for 30 mins in front. Di water applied here prevent the gas exchange between inner environment and outer environment, and so keeps the synthesized LFP form oxidizing by refilled oxidant. It collects the water vapor and purges out other gases. Since all gases purged out are air components, it is also works as an exhaust treatment component. The gas will keep flowing until an equilibrium of internal pressure and external pressure is reached during reaction. It should be noticed that after the reaction is done, during cooling

`

process (with lower temperature), the inner pressure will start to lower than the outer pressure base on the gas law. This will cause a reversed pressure gradient and lead to a backflow of Di water. Therefore, the valve is closed once the heating process is finished.

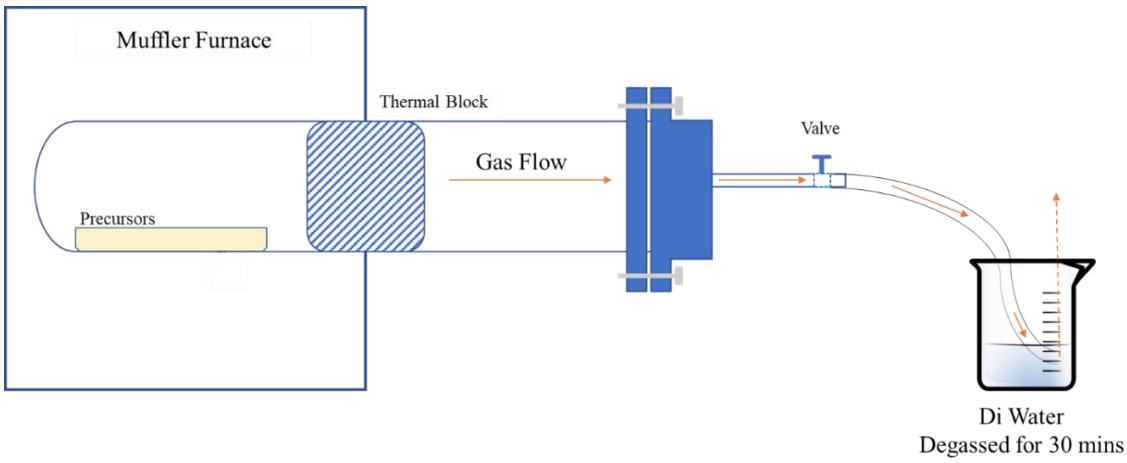

Figure 4.2. The schematic diagram for LFP synthesis setup

LFP is synthesized with experiment scale (0.6 g) and a larger scale (6 g) of precursors to investigate the system potential for scale-up synthesis. Then, a time study is done to understand the LFP synthesis process and optimize the reaction time.

Finally, in order to decrease the partial pressure of oxidant gas and so improve the quality of LFP, water is used as a sacrificial material to release extra amount of gases via its evaporation. As illustrate in Figure 4.3, another quartz boat which contains water is located next to the precursors boat. LFP synthesized with application of 2 g and 10 g of sacrificial materials are studied, respectively.

`

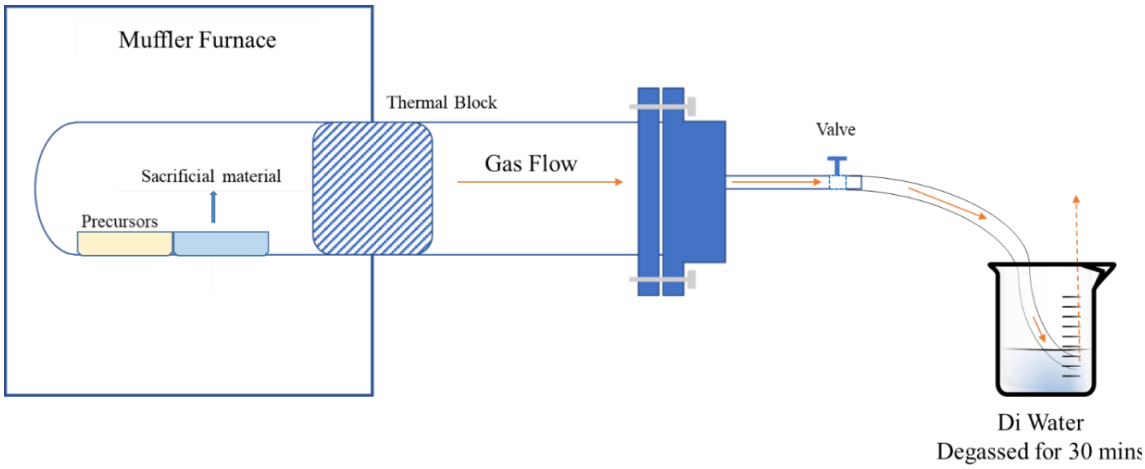

Figure 4.3. The schematic diagram for modified LFP synthesis setup

In this chapter, XRD was applied to analyze the crystalline phase of synthesized LFP. Raman is used to examine the carbonization rate of synthesized LFP.

4.3 Results and discussion

The XRD patterns for LFP synthesized with APR enhancement is demonstrated in Figure 4.4. The patterns for LFP synthesized without using of ARP is also demonstrated here for comparing. They are denoted as LFP-APR and LFP-CV. Both LFP-APR and LFP-CV have excellent crystallinity of LFP in compare to referenced LFP patterns. They also have similar significance on Li_3PO_4 and α-Fe_2O_3 peaks. These all demonstrate that LFP synthesized in these two conditions have nearly same quality. Here, the concern is the increasing on reaction temperature and time may accelerate the LFP oxidation process by O_2. However, with application of APR, part of the oxidant gases has flowed to the outside environment. This decrease the internal pressure for oxidant and according to Figure 4.4, it can offset the extra oxidation effect caused by temperature and time increment. Then, the main different between XRD patterns of LFP-APR and LFP-CV is the carbon peak

`

which is at 27° and denoted with a star. With 750 ℃ and long enough time (5 hours) applied, gelatin is completely decomposed and remain with the carbon [6]. With 20% of gelatin added in front, the carbon remained is about 10%. The referenced LFP has a carbon component of 1.1 to 1.5%. This is the reason that no carbon peak is observed in its XRD patterns. Existence of carbon is the necessary but not inadequate condition for a well formed LFP carbonization layer. Therefore, a Raman spectroscopy characterization is required to investigate the carbonization level of LFP.

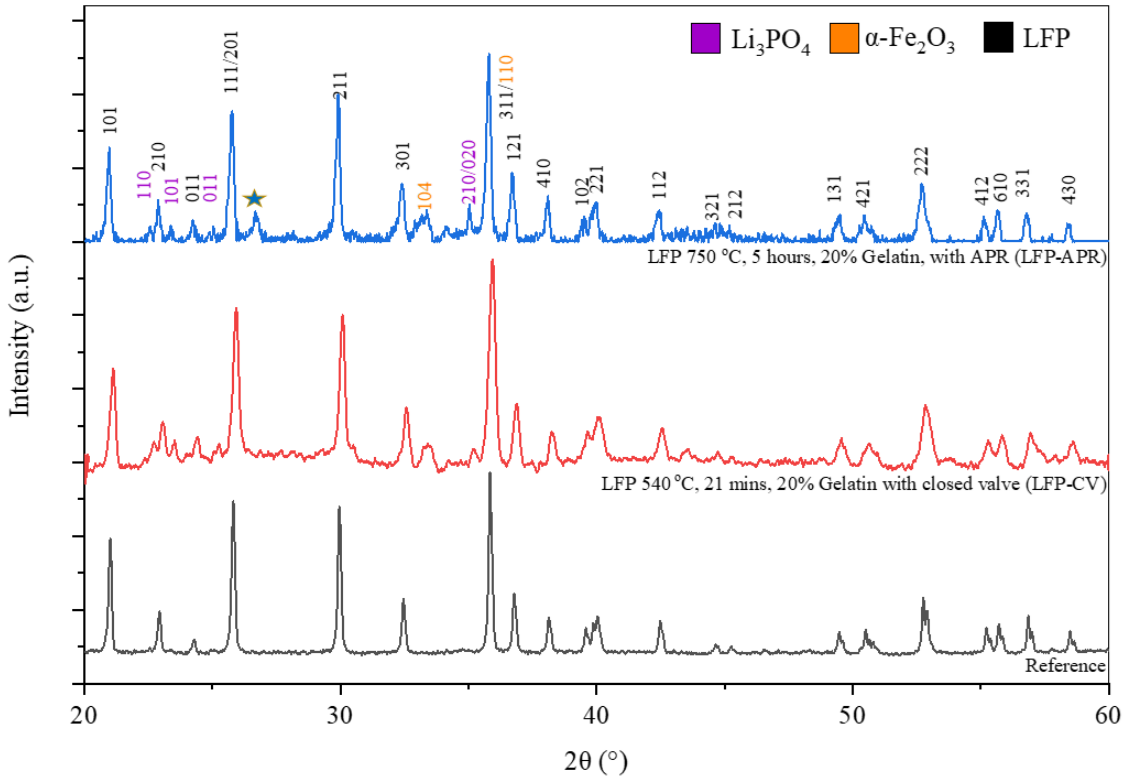

Figure 4.4. The XRD patterns for LFP-APR and LFP-CV

`

Figure 4.5 is the Raman spectroscopy result for LFP-APR. The peak at 1310 cm^{-1} and 1596 cm^{-1} are the D-band and G-band for carbon coating [7]–[10]. The intensity for D-band, G-band and the ratio between them are listed in Table 4.1. For carbon coating, G-band corresponds to graphitized structured carbon while D-band corresponds to disordered structured carbon [3]. The graphitized structured carbon has higher ionic and electronic conductivity than disordered carbon [11]. Since LFP-APR has a ratio of D-band verse G-band larger than one, it has a lower graphitization degree which represent a possible lower conductivity [12]. The oxidize environment in LFP-APR synthesis is the reason causes graphitization degree loss. On the other hand, the peak at 950 cm^{-1} demonstrates the PO_4^{3-} band for LFP. For carbonized LFP, because of the strong intensity for D-band and G-band, the peak intensity for bands in LFP is usually small. Thus, only PO_4^{3-} band at 950 cm^{-1} can usually be observed. It can be found that PO_4^{3-} band for LFP-APR has a lower intensity which almost merges into background signal. This is similar case in compare to Figure 4.4 which is caused by the higher carbon content of LFP-APR.

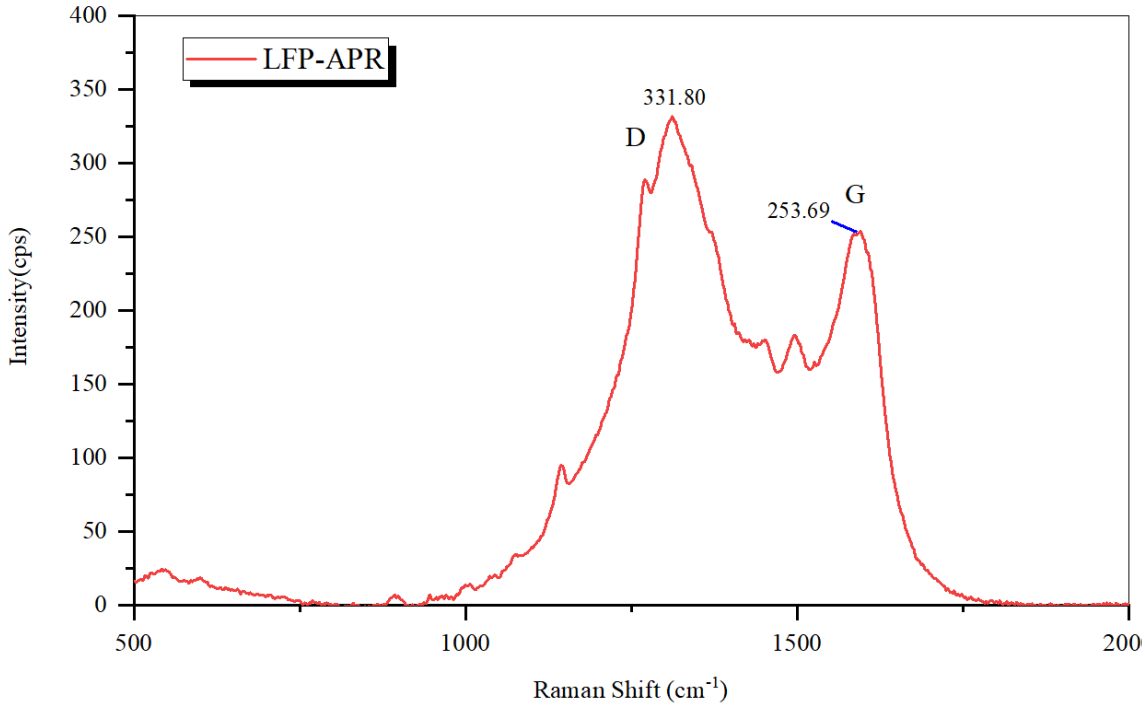

Figure 4.5. The Raman spectroscopy result for LFP-APR and LFP Reference

Table 4.1. The D and G-band for LFP-APR

Materials	Intensity of D-band (cps)	Intensity of G-band (cps)	Ratio (D:G)
LFP-APR	331.80	253.69	1.30

`

So far, the modifications have been taken allow the synthesis of LFP with same level quality and successful carbonization in compare to chapter 3. Then, LFP with larger scale is synthesized in same condition to examine potential to produce LFP in industry level. In compare to 0.6 g scale for precursors applied in pervious synthesis, a 10 times (6 g) weight of precursors, which is 10 times of stander scale, is used to synthesis LFP. The XRD patterns for these LFP is illustrated in Figure 4.6. It can be found LFP synthesized with 0.6 g of precursors and 6 g of precursors have nearly same XRD patterns. With all the experiment parameters unchanged, the only impact brought by the 6 g scale synthesis is amount of gases release. The released gas contains two parts:

(1) H_2O and CO_2 released by LFP synthesized reaction:

$$4FePO_4(s) + 4CH_3COOLi\ (s) \longrightarrow 4LiFePO_4\ (s) + 6H_2O\ (g) + CO_2\ (g) + 7C\ (s)$$

Thus, the weight percentage of gas released for this reaction is:

$$Wt\% = \frac{6\times N_{H_2O} + N_{CO_2}}{4\times N_{FePO_4} + 4\times N_{CH_3COOLi}} = 17.6\%$$

(2) Gas released via gelatin decomposition, according to the TGA result of gelatin, the weight loss in this process is 75%

`

With a 20wt% of gelatin added into precursors, the gas released in this case is 29%. With the scale changed from 0.6 g to 6 g, the extra gas released is 1.57 g. According to Figure 4.6, this different is not enough to cause significant XRD patterns change. The inner pressure of reaction chamber is remained stable since the released gases are kept purging out. This means the APR can efficiently balance the pressure with a larger scale of synthesis. It shows the potential to synthesis LFP in industry level without the need of enhancing pressure resistance for reaction chamber or applying a larger chamber for reaction.

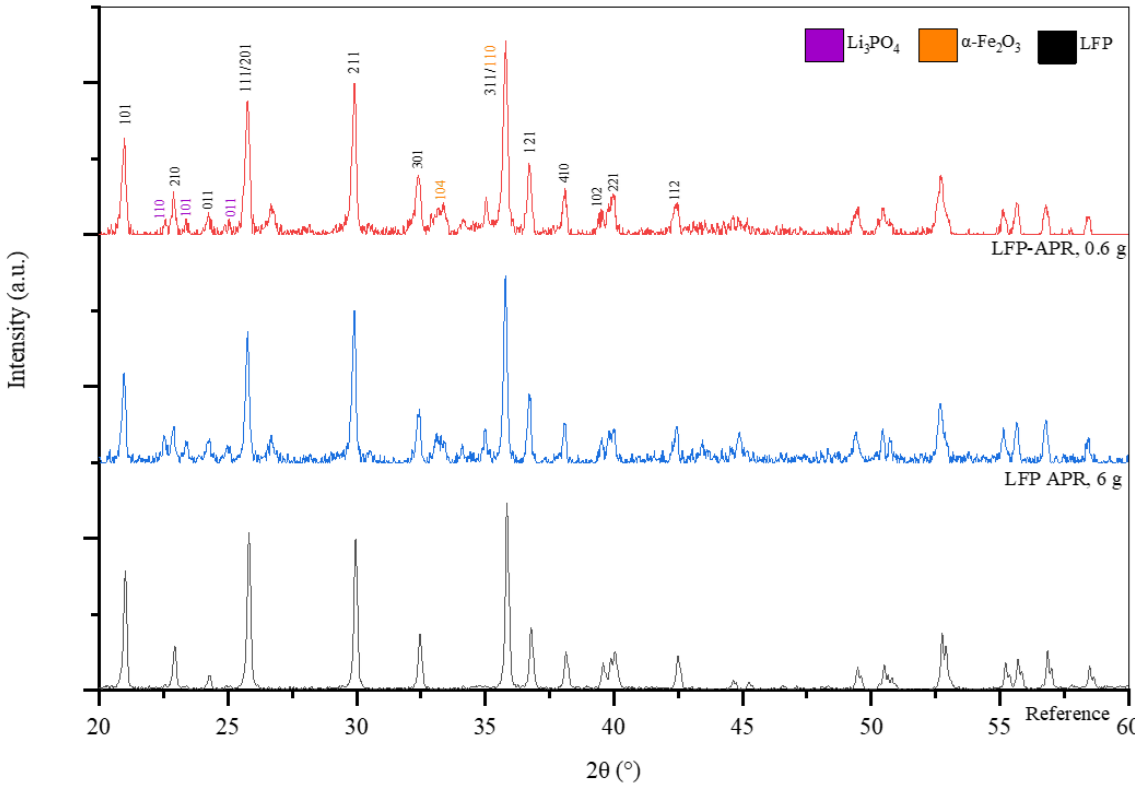

Figure 4.6.LFP-APR synthesized with 0.6 g and 6 g of precursors

`

The XRD patterns for LFP-APR synthesized in different time are demonstrated in Figure 4.7. LFP synthesized in 0 (which is the mixture of precursors) 2, 3, 4, 5, 10, 60 and 300 minutes are denoted as LFP-APR000, LFP-APR002, LFP-APR003, LFP-APR004, LFP-APR005, LFP-APR010, LFP-APR060 and LFP-APR300, respectively. All of them are synthesized with 20wt% of gelatin added. Featured with (012) and (100) peaks, the XRD patterns for the LFP-APR000 (precursors) are same to the XRD patterns of quartz $FePO_4$. LFP start to be yielded between 3 to 4 mins. Especially for LFP-APR004, (012) from $FePO_4$ and (111/201) from LFP have a peak overlapping which created a trapezoid peak around 26°. LFP-APR004 showed the early stage of LFP growth, the four most significant peaks for LFP, (101), (111/201), (211), and (311), start to show up. And the peaks for iron oxide (both α-Fe_2O_3 and γ-Fe_2O_3) also appear, though they have very low significance. The metastable γ-Fe_2O_3 is produced because of the high temperature and large thermal shock applied [13]. Over time, γ-Fe_2O_3 is firstly reduced by carbon and oxidized LFP is regenerated. And finally in LFP-APR300, the (220) peak for γ-Fe_2O_3 is completely disappeared.

Then, looking at LFP-APR005, it is found that the peaks for carbon appears. As discussed in Chapter 3, the degradation process of gelatin releases carbon at relatively low temperature in compare to lithium acetate. Therefore, it can inhibit the oxidation reaction and limited oxidation at certain level. The carbon formed at beginning stage of oxidation has proved its ability to improve the quality of LFP. A more cleared peaks for LFP can be observed in LFP-APR010. The peaks here are more significant in intensity. This XRD patterns is consistent with the result demonstrated in Figure 3.10, LFP09.

`

LFP-APR060 has already showed a XRD patterns for high quality LFP. Its patterns are almost same to LFP-APR-300. Meaning current reaction time has a great potential to be optimized. The 5 hours applied for LFP synthesis is an excess value to ensure the completion of reaction and carbon coating. The XRD patterns for LFP-APR060 may indicate the actual time needed for this approach can be less than 1 hour which is far shorter than conventional solid state LFP synthesis [14]–[16].

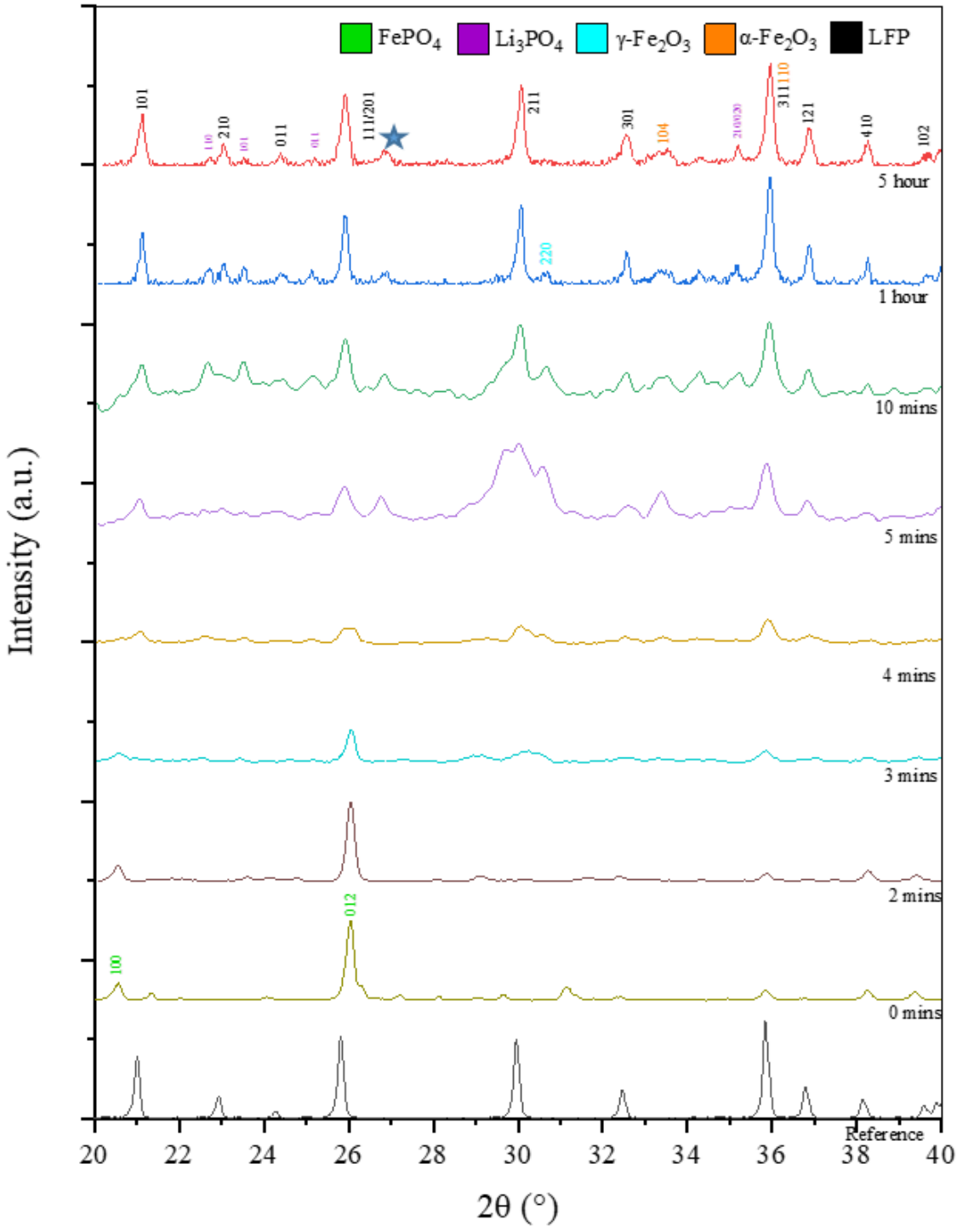

Figure 4.7. XRD pattern for LFP-APR synthesized in different time

`

Currently, the only issue remained is to decrease the partial pressure of oxygen inside the reaction chamber and so improve the quality of LFP. LFP synthesized with using 2 g and 10 g of water as sacrificial material is characterized by XRD and demonstrated in Figure 4.8. LFP-APR and LFP reference are also included for comparison. There is no significant change between the XRD patterns of LFP-APR and LFP synthesized with 2 g of water. Again, it proved that certain amount the sacrificial material is required to influence the quality of LFP. A much more significant change can be observed in LFP synthesized with 10 g of water. The LFP in this case is well crystallized and contains less impurities in compare to LFP-APR. The peaks for Li_3PO_4 are nearly merged into background patterns. Also, the Fe_2O_3 peak also reaches the lowest significant among all the LFP synthesized in this dissertation. The modification of using water as sacrificial material played a critical role in LFP synthesis in an unrestricted environment. It successfully increases the inner pressure of reaction chamber during LFP synthesis. Then, while the gases flowing to the outside environment, a significant amount of oxygen originally existed inside the reaction chamber has also been purged out. With a result of the lower partial pressure for oxygen, the oxidation of LFP is limited at a lower level associated with less yielding of Li_3PO_4.

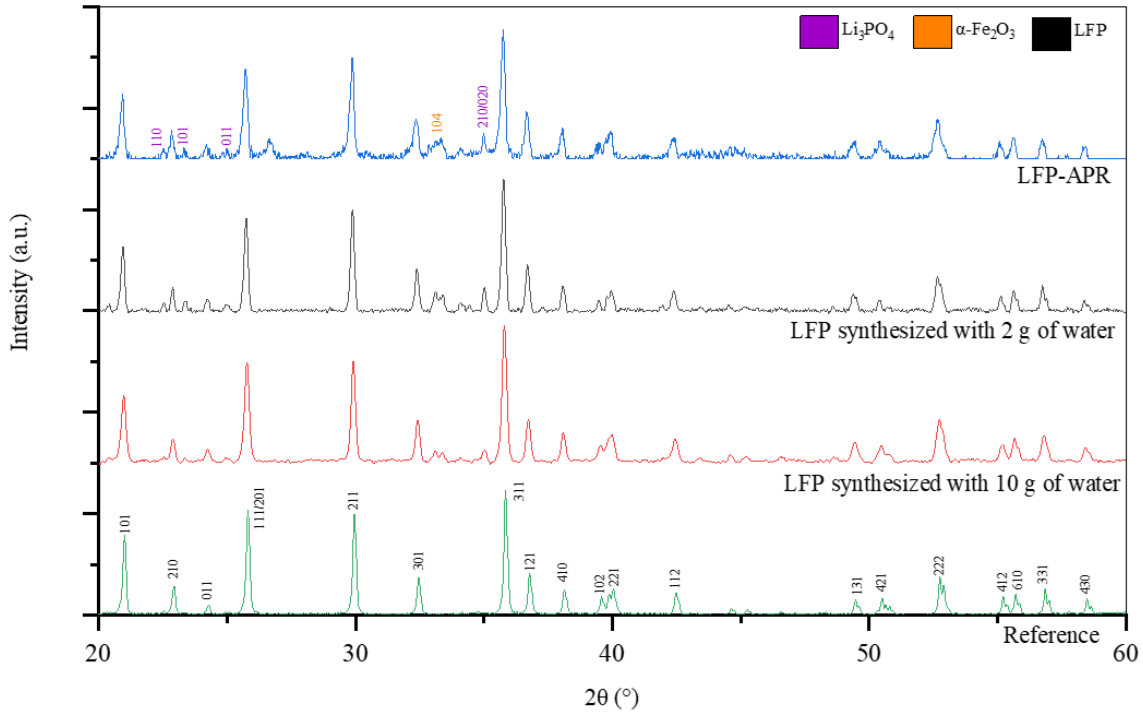

Figure 4.8. XRD patterns for LFP-WR, LFP synthesized with 2 g of water and LFP synthesized with 10 g of water

`

The high quality of LFP is then confirmed by FTIR which is demonstrated in Figure 4.9. For LFP, two groups of transmittance peaks are considered: (1) High wavenumber peaks which are related to the stretching and vibration of PO_4^{3+}; (2) Low wavenumber peaks which are related to the Li^+ environment. Both peaks for LFP synthesized with 10 g of water are matched with referenced LFP. Furthermore, no impurity peaks are observed in synthesized LFP. This result is consistent with the XRD patterns demonstrated in Figure 4.8 and supports the conclusion that LFP synthesized in this case has nice quality and limited impurity.

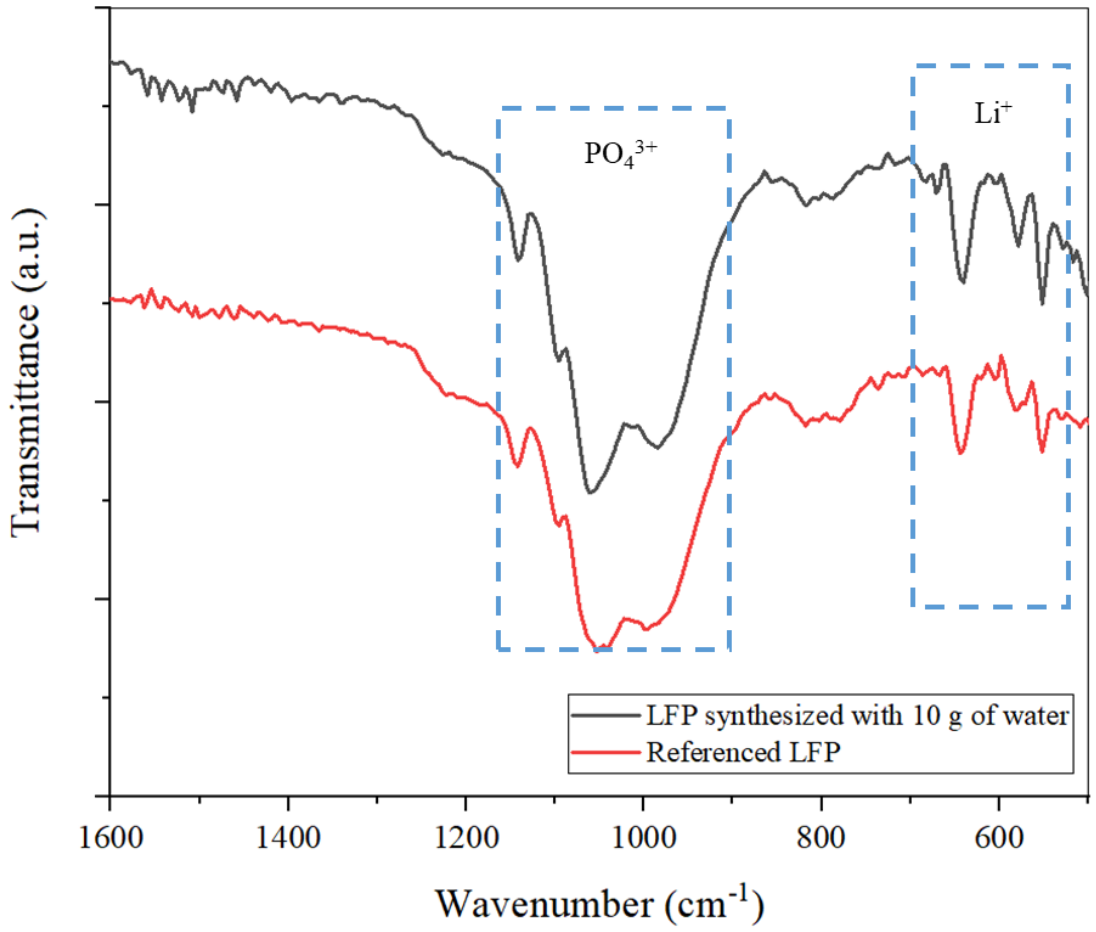

Figure 4.9. The FTIR result for LFP synthesized with 10 g of water and reference LFP

`

The morphology of the LFP synthesized with 10 g of water is characterized by SEM. An EDS is used at the same time to achieve the element distribution information of synthesized LFP. Demonstrated in Figure 4.10 (a), the LFP synthesized has a particle size distribution from hundreds nanometers to several micrometers. The wide distribution of size can be contributed to the wide distribution of precursors materials, especially quartz $FePO_4$. Figure 4.10 (b) and (c) are the element map for P and Fe, respectively. The distribution of element P and Fe are consistent with each other. No significant element cluster is observed, which indicates the phase of Fe_2O_3 and Li_3PO_4 are limited at low level. It confirms with the results of XRD and FTIR.

`

(a)

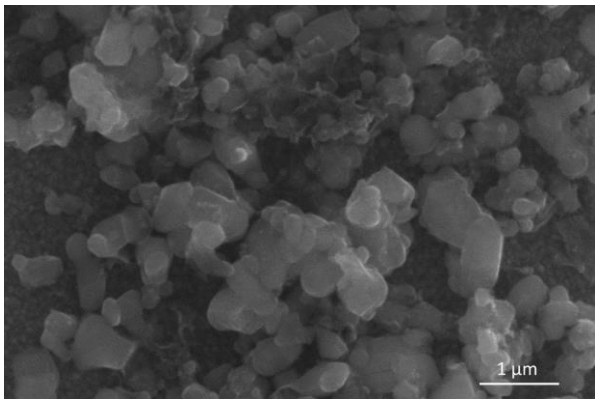

(b)

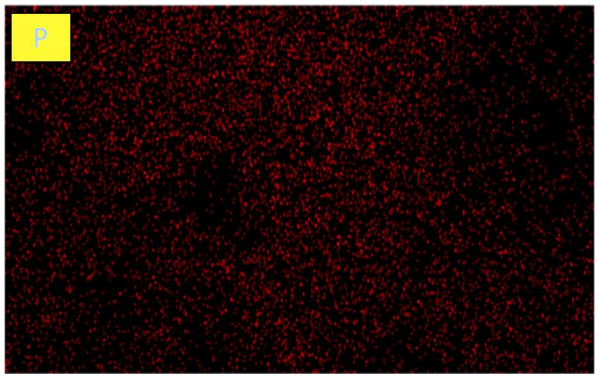

(c)

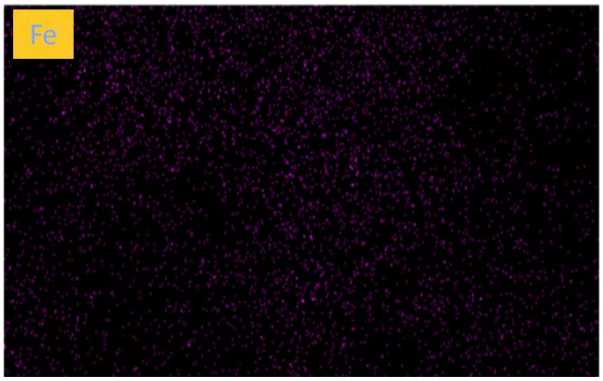

Figure 4.10. The (a) SEM image (b) element P distribution and (c) element Fe distribution for LFP synthesized with 10 g of water

`

The volume of reaction chamber is about 0.5 L. It contains about 0.02 mol of air. In the case of applying 10 g of water (0.56 mol) as sacrificial materials, the gases originally inside the chamber and the gases released by the precursors is negligible. Using Van der Waals model for real gas [17] and the following equation can be achieved:

$$(P-\frac{aN^2}{V^2})(V-Nb) = NRT$$

Where, P is the inner pressure, V is the volume of reaction chamber (0.5 L), N is the mole number of gas which is water vapor here, R is the ideal gas constant, T is the temperature the water vapor starts to flow which is assume to be slightly higher than the boiling point of water, 400 K. a and b are parameters that are determined empirically. With $a_{H_2O}=0.555\ J\cdot m^3\cdot mol^{-2}$, and $b_{H_2O}=3.06\times10^{-5}\ m^3\cdot mol^{-1}$, when the inner pressure and outer pressure reach an equilibrium, the inner pressure is equal to 1 atm. So the equation above can be written in SI unit in following form:

$$(1\times10^5\ kg\cdot m^{-1}\cdot s^{-2}-\frac{0.555\ kg\cdot m^5\cdot s^{-2}\cdot mol^{-2}\times N^2}{(5\times10^{-4}\ m^3)^2})(5\times10^{-4}\ m^3-3.06\times10^{-5}\ m^3\cdot mol^{-1}\cdot N)$$
$$=N\times8.314\ kg\cdot m^{-1}\cdot s^{-2}\cdot mol\cdot K^{-1}\times400\ K$$

Then a function of N is achieved:

$$(1-22N^2)(50-3N)=3326N$$

Thus, we have N = 0.015 mol. In compare to 0.56 mol of water used as sacrificial material, the gas remained in chamber is 2.7% in mole after reach of pressure equilibrium. Assuming each gas molecular is purged out with equal opportunity, so at maximum, 97.3% of oxygen can be removed from chamber via flow created by this 10 g of water. The thing limits the

`

percentage of oxygen that can flow to the outside environment to reach its maximum is temperature gradient as demonstrated in Figure 4.11. The temperature on the outside of thermal block decrease significantly and it is almost equal to the room temperature in rubber catheter. Water vapor can liquefy before flow into the water recycle system. The liquefaction mitigates the driving force of gas flow caused by pressure gradient. And this is the reason that using 2 g of water as sacrificial material gets very little effect on improving LFP quality. Certain amount of water, such as 10 g used in this research, is required to purge out part of oxygen. Materials which is volatile (acetone) or releases room temperature gas (CO_2) will be more efficient on purging out oxygen. However, considered the cost effectiveness, environmental friendliness, and reusability, water is still the first choice.

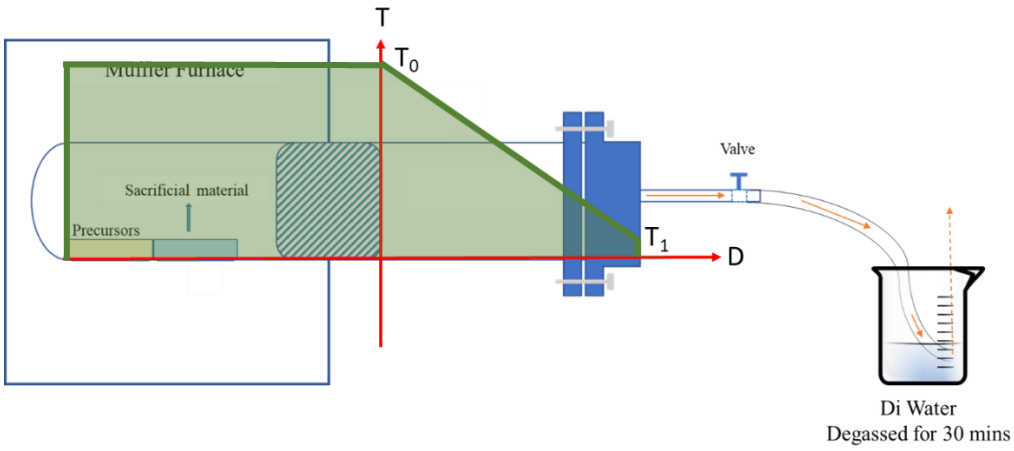

Figure 4.11. The schematic diagram of temperature gradient in reaction chamber

`

The LFP synthesized with 10 g of water is then characterized via a Raman spectroscopy to investigate the carbonization level. The result is demonstrated in Figure 4.12 and the information of D and G-band are listed in Table 4.2. According to the result, the LFP synthesized with 10 g of water has a D-band verse G-band ratio of 1.21, which means its graphitization degree is still lower than disorder level. There is more disordered carbon contained in the LFP than graphitized carbon. However, it still has higher graphitization level than LFP-APR because of its better LFP quality. It should be noticed Raman can characterize the carbon state in LFP, but if a uniform carbon coating is formed need to be investigated via TEM.

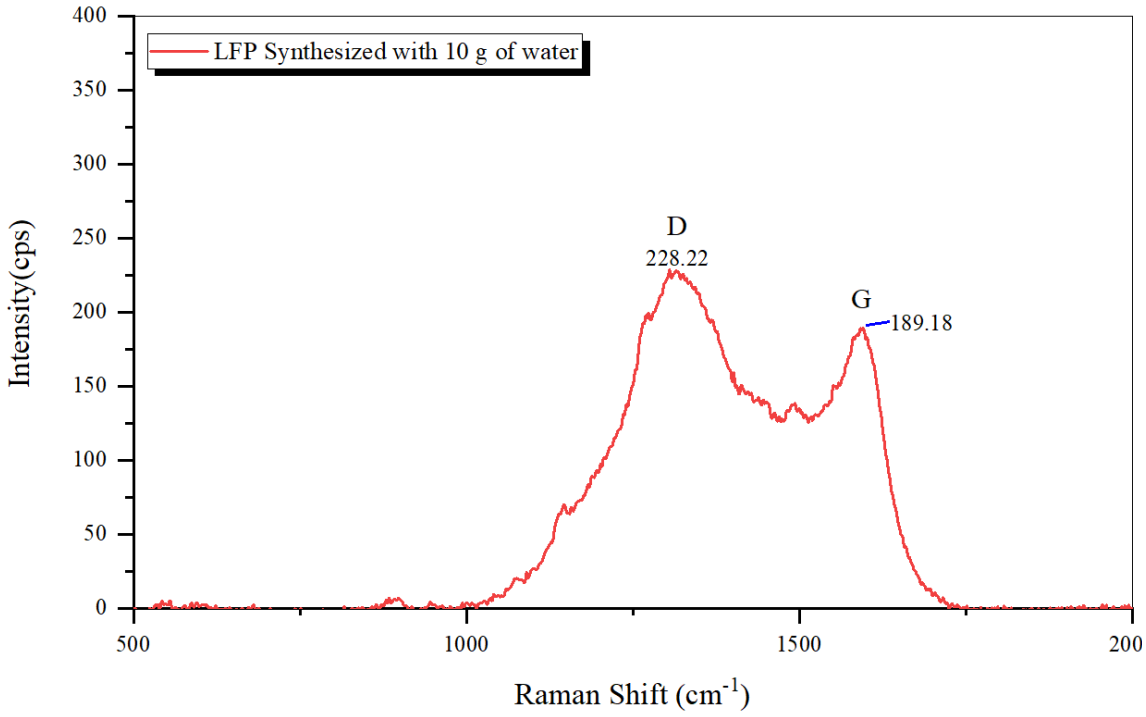

Figure 4.12. The Raman spectroscopy result for LFP synthesized with 10 g of water and LFP Reference

Table 4.2. The D and G-band for LFP synthesized with 10 g of water and LFP Reference

Materials	Intensity of D-band (cps)	Intensity of G-band (cps)	Ratio (D:G)
LFP synthesized with 10 g of water	228.22	189.18	1.21

`

Therefore, LFP synthesized with 10 g of water is then characterized by HR-TEM and TEM which are demonstrated in Figure 4.13. A clear pattern for carbon in (011) direction can be observed by HR-TEM in Figure 4.13 (a). The layer distance for this graphitized carbon is 0.37 nm. Carbon forms a coating layer and covers synthesized LFP particles. A more clear view of coated LFP can be observed via TEM in Figure 4.13 (b). Here, a uniform carbon coating layer with a coating thickness about 20 nm is observed. The uniformed coating can enhance the electric and ionic conductivity of LFP.

`

(a)

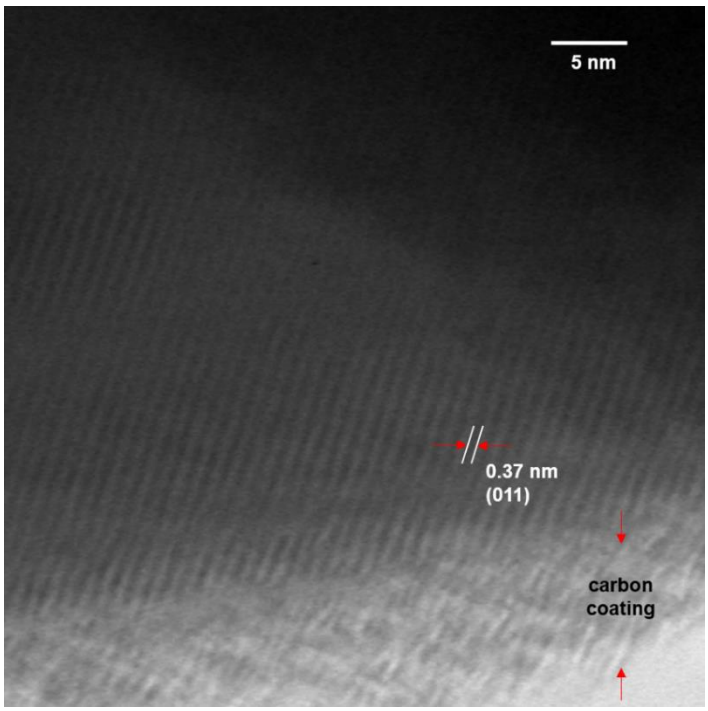

(b)

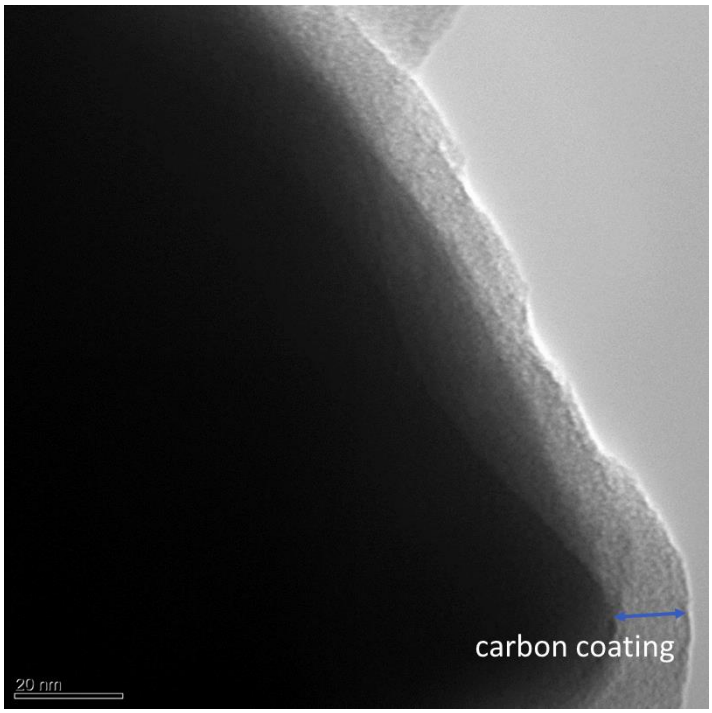

Figure 4.13. The (a)HR-TEM and (b)TEM image for LFP synthesized with 10 g water

`

4.4 Conclusion

In this chapter, in order to carbonize LFP to improve its electric and ionic conductivity, a higher reaction temperature and longer reaction time is applied. Then, by utilizing a newly added APR, the quality of LFP can also be maintained under these synthesis conditions. APR also shade some light on scale-up synthesis for LFP via lithation in an unrestricted environment because it can balance the inner and out pressure and let them reach an equilibrium during synthesis.

In order to further improve the quality of synthesized LFP, here, the pressure balance process is utilized to purge out part of oxygen. With application of 10 g of water as sacrificial material, finally, crystalline LFP/C with lower impurity rate is acquired.

`

Reference:

[1] J. Li, W. Yao, S. Martin, and D. Vaknin, “Lithium ion conductivity in single crystal LiFePO4,” *Solid State Ionics*, vol. 179, no. 2008, pp. 2016–2019, 2008.

[2] X. Zhi, G. Liang, L. Wang, X. Ou, L. Gao, and X. Jie, “Optimization of carbon coatings on LiFePO 4 : Carbonization temperature and carbon content,” *J. Alloys Compd.*, vol. 503, no. 2, pp. 370–374, 2010.

[3] V. Gariépy *et al.*, “Effect of the Carbonization on the LiFePO4 Particles of Positive Electrode for Rechargeable Lithium Batteries,” *ECS Trans.*, vol. 58, no. 14, pp. 73–78, 2014.

[4] M. Cuisinier, J. Martin, N. Dupré, A. Yamada, R. Kanno, and D. Guyomard, “Electrochemistry Communications Moisture driven aging mechanism of LiFePO4 subjected to air exposure,” *Electrochem. commun.*, vol. 12, no. 2, pp. 238–241, 2010.

[5] K. Zaghib *et al.*, “Aging of LiFePO4 upon exposure to H2O,” *J. Power Sources*, vol. 185, pp. 698–710, 2008.

[6] P. L. M. Barreto, A. T. N. Pires, and V. Soldi, “Thermal degradation of edible films based on milk proteins and gelatin in inert atmosphere,” *Polym. Degrad. Stab.*, vol. 79, pp. 147–152, 2003.

[7] J. Nanda *et al.*, “Thermophysical properties of LiFePO 4 cathodes with carbonized pitch coatings and organic binders : Experiments and fi rst-principles modeling,” *J. Power Sources*, vol. 251, pp. 8–13, 2014.

[8] E. Golestani, M. Javanbakht, and H. Ghafarian-zahmatkesh, “Electrochimica Acta Tartaric acid assisted carbonization of LiFePO4 synthesized through in situ hydrothermal process in aqueous glycerol solution,” *Electrochim. Acta*, vol. 259, pp. 903–915, 2018.

[9] J. S. Park, A. Reina, R. Saito, J. Kong, G. Dresselhaus, and M. S. Dresselhaus, “G band Raman spectra of single , double and triple layer graphene,” *Carbon N. Y.*, vol. 47, no. 5, pp. 1303–1310, 2009.

[10] M. J. Matthews and M. A. Pimenta, “Origin of dispersive effects of the Raman D band in carbon materials,” *Phys. Rev. B*, vol. 59, no. 10, pp. 6585–6588, 1999.

[11] X. Zhang, D. Liu, L. Yang, L. Zhou, and T. You, “Self-assembled three-dimensional graphene-based materials for dye adsorption and catalysis,” *J. Mater. Chem. A*, vol. 3, pp. 10031–10037, 2015.

[12] X. Yang, F. Mou, L. Zhang, G. Peng, Z. Dai, and Z. Wen, “Enhanced rate performance of two-phase carbon coated LiFePO 4 /(C + G) using natural graphite as carbon source,” *J. Power Sources*, vol. 204, pp. 182–186, 2012.

[13] G. Schimanke and M. Martin, “In situ XRD study of the phase transition of

nanocrystalline maghemite (γ-Fe2O3) to hematite (α-Fe2O3)," *Solid State Ionics*, vol. 136, no. 137, pp. 1235–1240, 2000.

[14] P. Benedek, N. Wenzler, M. Yarema, and V. C. Wood, "Low temperature hydrothermal synthesis of battery grade lithium iron phosphate," *RSC Adv.*, vol. 7, no. 29, pp. 17763–17767, 2017.

[15] C. H. Mi, G. S. Cao, and X. B. Zhao, "Low-cost , one-step process for synthesis of carbon-coated LiFePO4 cathode," *Electrochim. Acta*, vol. 59, pp. 127–130, 2005.

[16] T. V. S. L. Satyavani, A. Srinivas Kumar, and P. S. V. Subba Rao, "Methods of synthesis and performance improvement of lithium iron phosphate for high rate Li-ion batteries: A review," *Eng. Sci. Technol. an Int. J.*, vol. 19, no. 1, pp. 178–188, 2016.

[17] P. Colonna and A. Guardone, "dynamics of dense vapors under the van der," *Phys. Fluids*, vol. 18, no. 056101, 2006.

`

Chapter 5 Conclusion of dissertation

In order to synthesis high quality LFP in a cost effective, energy effective and environmental friendly way, a lithation in an unrestricted environment is developed. This approach is developed base on conventional solid state approach and it is conducted in a closed chamber. It uses $FePO_4$ as iron source and lithium acetate as lithium source. The crystal structure of $FePO_4$ which is depended on the dehydration temperature of $FePO_4$ significantly impact the quality of LFP. On the other hand, using lithium acetate accelerates the reaction rate. As result in Chapter 2, by using quartz $FePO_4$, and lithium acetate, crystalline LFP can be synthesized in short time in compare to conventional solid state synthesis.

The biggest challenge for synthesizing LFP in an unrestricted environment is the oxidation of LFP. Therefore, in Chapter 3, gelatin is added into precursors as a carbon source. The carbon released via gelatin thermal decomposition perform as sacrificial material which consume the oxygen and an agent of reduce which regenerates oxidized LFP. Using gelatin successfully limited the oxidation in a certain level and improve the quality of synthesized LFP. However, there are two issues remained: (1) with a closed chamber used for reaction, the scale that LFP can be produced is limited. This is due to the gases released during LFP synthesis reaction can increase the inner pressure for chamber. The higher inner pressure puts forward higher requirements on reaction chamber, especially on pressure resistance or requires using of a larger chamber. (2) LFP need to be carbonized to improve its electric and ionic conductivity.

`

Therefore, in Chapter 4, reaction temperature and time is adjusted to fulfil the requirement of carbonization. And more importantly, a APR is developed and added in to the pervious experiment setting. The new system allows the inner gas flow to the outer environment and so let the inner pressure and outer pressure reach to an equilibrium. This mitigates the pressure brought by the produced gases and then makes the large scale synthesis of LFP possible.

Finally, extra water contained in a separate quartz boat is utilized as a sacrificial material to be placed inside the chamber via heating. It is evaporated during LFP synthesis and significantly increases the amount of gases inside chamber. While the gases flow to the outer environment, the partial pressure of oxygen is successfully decreased. As a final result, LFP/C with high quality and minimum impurity is synthesized.